Nuclear and neutron matter G-matrix calculations with a chiral effective field theory potential including effects of three-nucleon interactions

M. Kohno (河野通郎)*
Physics Division, Kyushu Dental University, Kitakyushu 803-8580, Japan
(Received 18 September 2013; published 30 December 2013)

The energies of symmetric nuclear matter and neutron matter are evaluated in the lowest-order Brueckner theory using a chiral effective field theory potential including effects of a three-nucleon force (3NF). The 3NF is first reduced to a density-dependent nucleon-nucleon (NN) force by folding with single-nucleon degrees of freedom in infinite matter. Adding the reduced NN force to the initial NN force and applying a partial-wave expansion, G-matrix calculations are performed in pure neutron matter as well as in symmetric nuclear matter. A saturation curve which is close to the empirical one is obtained. It is explicitly shown that the cutoff-energy dependence of the calculated energies is substantially reduced by including the 3NF. Characteristics of 3NF contributions in separate spin and isospin channels are discussed. Calculated energies of neutron matter are very similar to those employed in the literature for considering neutron star properties.

DOI: 10.1103/PhysRevC.88.064005 PACS number(s): 21.30.Fe, 21.65.Cd, 21.65.Mn, 26.60.Kp

I. INTRODUCTION

One of the basic goals in nuclear physics is to understand characteristic properties of nuclei, especially the saturation and the single-particle shell structure, starting from underlying nucleon-nucleon (NN) interactions. Various many-body theories have been developed since the 1950s. Brueckner theory [1–3], which was initiated from a multiple-scattering viewpoint and later established as the linked-cluster expansion in terms of G matrices, has served as a standard method to understand nuclei as a system of nucleons moving independently in a mean field in spite of the NN interactions having singularly strong repulsion in the short-distance region. Another basic method for treating quantum many-body problems is a variational approach [4], although the shell structure is not intuitive in this framework. Two methods in a nonrelativistic framework are now known to provide a similar description of nuclear bulk properties [5]. These results unfortunately indicate that the saturation cannot be correctly reproduced in a nonrelativistic framework when realistic NN potentials are used. Various elaborate many-body methods utilized in recent years, such as the coupled-cluster method, the unitary correlated basis method, and the no-core shell model with low-momentum interactions, confirm this situation.

Various attempts have been made to include other mechanisms to improve the description of the saturation properties, such as relativistic effects and three-nucleon force (3NF) contributions in the nuclear medium. It was demonstrated that relativistic Brueckner-Hartree-Fock calculations [6] can provide a satisfactory saturation curve. However, because contributions from higher-order correlations and three-nucleon forces have not been fully estimated in the relativistic treatment, the problem seems not to be settled yet. In the last decade, a new description of the NN potential has been developed [7–9]; that is, the interaction based on chiral effective field theory (Ch-EFT). The potential form is dictated by the underlying chiral symmetry of the QCD, and potential parameters, low-energy constants, are adjusted to explain scattering data as in other realistic NN potentials. 3NFs are systematically introduced in this framework and most parameters in these terms are taken over from the NN sector.

The introduction of 3NFs has a long history starting in the 1950s, and numerous studies have been devoted to 3NF contributions in nuclear properties. Besides three-body correlations through ordinary NN forces, 3NFs may arise from excitations of virtual nucleon-antinucleon pairs as well as the Δ isobar and other nucleon excited states in the medium [10,11]. The importance of 3NFs, in the standard nonrelativistic description of nuclei, has been established by precise few-body calculations [12,13]. It has also been recognized that 3NFs are necessary to reproduce empirical saturation properties [5,14–16]. Regardless of the fact that numerical calculations that reproduce nuclear saturation properties by including 3NF effects have been presented by various authors, the advantage of using the Ch-EFT is that the contribution of the 3NF can be discussed in a systematic way consistent with the initial NN interaction.

Some perturbative considerations for neutron matter properties with the Ch-EFT interaction including the 3NF have been reported in Refs. [17–21]. The present author gave, in Ref. [22], a brief report on the lowest-order Brueckner theory (LOBT) calculation in nuclear matter using the reduced density-dependent NN force obtained from the Ch-EFT 3NF, in which a focus was put on the effective spin-orbit strength. Similar LOBT calculations also appeared in Ref. [23].

In this paper, I report, in detail, nuclear and neutron matter calculations in LOBT based on the N^{3}LO Ch-EFT potential including its N^{2}LO 3NF. Because the Ch-EFT is a definite way to organize the interaction between nucleons, it is important to study the implication of the interaction based on it to the nuclear many-body problem. However, it is presently impossible to consider full contributions of 3NFs together with many-body correlations, except for very light nuclei. Even for the NN force, it is already very difficult to take into account effects of more than three-nucleon

*kohno@kyu-dent.ac.jp

correlations. Therefore, we introduce an approximation. First, reduced effective NN forces are constructed by averaging the 3NF over the third nucleon in the Fermi sea. Adding the reduced NN force to the initial Ch-EFT NN interaction, we carry out standard G-matrix calculations. This procedure may not be accommodated rigorously in a linked-cluster expansion of quantum many-body theory. Nevertheless, we should expect meaningful information about the role of 3NFs in this estimation.

The procedure for including the reduced NN force from the Ch-EHF 3NF in LOBT calculations is explained in Sec. II. For numerical calculations in a standard method, it is necessary to introduce a partial-wave expansion of the reduced NN interaction. This is straightforward but somewhat intricate. Explicit expressions of the reduced NN interaction are given in Appendix A. Expressions after the partial-wave expansion are shown in Appendix B. Numerical results are presented first for nuclear matter in Sec. III, and then for neutron matter in Sec. IV. The cutoff-energy dependence of the calculated energies is demonstrated in these sections. A summary follows in Sec. V.

II. G MATRIX INCLUDING REDUCED NN FORCE FROM 3NF

It is difficult to treat the 3NF V_{123} directly in infinite matter. In this paper, I introduce an approximation of reducing the 3NF to an effective NN force by folding single-nucleon degrees of freedom, as has been often employed in the literature [14,15,24,25]. That is, the density dependent NN interaction $V_{12(3)}$ is defined, in momentum space, by the following summation over the third nucleon in the Fermi sea of nuclear matter:

$$\begin{aligned}&\langle \boldsymbol{k}_1'\sigma_1'\tau_1', \boldsymbol{k}_2'\sigma_2'\tau_2'|V_{12(3)}|\boldsymbol{k}_1\sigma_1\tau_1, \boldsymbol{k}_2\sigma_2\tau_2\rangle_A \\ &\quad\equiv \sum_{\boldsymbol{k}_3,\sigma_3\tau_3} \langle \boldsymbol{k}_1'\sigma_1'\tau_1', \boldsymbol{k}_2'\sigma_2'\tau_2', \boldsymbol{k}_3\sigma_3\tau_3| \\ &\qquad\times V_{123}|\boldsymbol{k}_1\sigma_1\tau_1, \boldsymbol{k}_2\sigma_2\tau_2, \boldsymbol{k}_3\sigma_3\tau_3\rangle_A. \end{aligned} \tag{1}$$

The suffix A denotes an antisymmetrized matrix element, namely $|ab\rangle_A \equiv |ab - ba\rangle$ and $|abc\rangle_A \equiv |abc - acb + bca - bac + cab - cba\rangle$. The remaining two nucleons are supposed to be in a center-of-mass frame; $\boldsymbol{k}_1' + \boldsymbol{k}_2' = \boldsymbol{k}_1 + \boldsymbol{k}_2 = 0$. We do not include the three-body form factor in this folding procedure, but introduce it later in the reduced NN interaction. In this case, matrix elements and their partial wave expansion can be carried out analytically for the Ch-EFT 3NF, as shown in Appendix A.

The necessity of taking into account correlations being neglected, contributions of the two- and three-nucleon forces, V_{12} and V_{123}, to the energy are given by

$$\begin{aligned}&\frac{1}{2}\sum_{\boldsymbol{k}_1\boldsymbol{k}_2}\langle \boldsymbol{k}_1\boldsymbol{k}_2|V_{12}|\boldsymbol{k}_1\boldsymbol{k}_2\rangle_A + \frac{1}{3!}\sum_{\boldsymbol{k}_1\boldsymbol{k}_2\boldsymbol{k}_3}\langle \boldsymbol{k}_1\boldsymbol{k}_2\boldsymbol{k}_3|V_{123}|\boldsymbol{k}_1\boldsymbol{k}_2\boldsymbol{k}_3\rangle_A \\ &\quad= \frac{1}{2}\sum_{\boldsymbol{k}_1\boldsymbol{k}_2}\langle \boldsymbol{k}_1\boldsymbol{k}_2|V_{12} + \frac{1}{3}V_{12(3)}|\boldsymbol{k}_1\boldsymbol{k}_2\rangle_A. \end{aligned} \tag{2}$$

This implies that the G matrix may be defined by

$$G_{12} = V_{12} + \frac{1}{3}V_{12(3)} + \left(V_{12} + \frac{1}{3}V_{12(3)}\right)\frac{Q}{\omega - H}G_{12}, \tag{3}$$

where Q stands for the Pauli exclusion operator and the denominator $\omega - H$ of the propagator is prescribed below. The similar evaluation of the single-particle energy needs a different combination factor:

$$\begin{aligned}&\langle \boldsymbol{k}|t|\boldsymbol{k}\rangle + \sum_{\boldsymbol{k}'}\langle \boldsymbol{k}\boldsymbol{k}'|V_{12}|\boldsymbol{k}\boldsymbol{k}'\rangle_A + \frac{1}{2}\sum_{\boldsymbol{k}'\boldsymbol{k}''}\langle \boldsymbol{k}\boldsymbol{k}'\boldsymbol{k}''|V_{123}|\boldsymbol{k}\boldsymbol{k}'\boldsymbol{k}''\rangle_A \\ &\quad= \langle \boldsymbol{k}|t|\boldsymbol{k}\rangle + \sum_{\boldsymbol{k}'}\langle \boldsymbol{k}\boldsymbol{k}'|V_{12} + \frac{1}{2}V_{12(3)}|\boldsymbol{k}\boldsymbol{k}'\rangle_A, \end{aligned} \tag{4}$$

where t is a kinetic-energy operator. It is reasonable to define the single-particle energy which is utilized in the denominator of the G-matrix equation, Eq. (3), employing the continuous prescription for intermediate states as

$$e_{\boldsymbol{k}} = \langle \boldsymbol{k}|t|\boldsymbol{k}\rangle + U_G(\boldsymbol{k}) \tag{5}$$

$$U_G(\boldsymbol{k}) \equiv \sum_{\boldsymbol{k}'}\langle \boldsymbol{k}\boldsymbol{k}'|G_{12} + \frac{1}{6}V_{12(3)}\left(1 + \frac{Q}{\omega - H}\right)G_{12}|\boldsymbol{k}\boldsymbol{k}'\rangle_A, \tag{6}$$

supposing that the effect of the NN correlation is approximated by that of the G-matrix equation. To be specific, the denominator $\omega - H$ in the G-matrix equation for $G|\boldsymbol{k}_1\boldsymbol{k}_2\rangle$ is given by $e_{\boldsymbol{k}_1} + e_{\boldsymbol{k}_2} - (t_1 + U_G(\boldsymbol{k}_1') + t_2 + U_G(\boldsymbol{k}_2'))$, where $\boldsymbol{k}_1'$ and $\boldsymbol{k}_2'$ are momenta of intermediate nucleons.

Solving the G-matrix equation together with the denominator explained above, the total energy is evaluated by

$$E = \sum_{\boldsymbol{k}}\langle \boldsymbol{k}|t|\boldsymbol{k}\rangle + \frac{1}{2}\sum_{\boldsymbol{k}}U_E(\boldsymbol{k}), \tag{7}$$

$$U_E(\boldsymbol{k}) = \sum_{\boldsymbol{k}'}\langle \boldsymbol{k}\boldsymbol{k}'|G_{12}|\boldsymbol{k}\boldsymbol{k}'\rangle_A. \tag{8}$$

The difference between $U_G(\boldsymbol{k})$ for the energy calculation and $U_E(\boldsymbol{k})$ appearing in the single-particle energy is a prototype of rearrangement energy. Naturally, the above treatment of the 3NF is heuristic. It is desirable to develop a more rigorous and systematic perturbative treatment. One possible framework may be a coupled cluster method, which was discussed in Ref. [26].

In actual calculations in nuclear matter, a partial wave expansion [27] is introduced with an angle-average approximation for the Pauli exclusion operator Q. The good quality of this approximation has been examined in the literature [28]. The partial wave expansion of the reduced NN interaction, Eq. (1), is carried out in a standard way, which may be found in the paper by Fujiwara *et al.* [29]. Partial waves up to the total angular momentum $J = 7$ and the orbital angular momentum $\ell = 7$ are included in numerical calculations.

For completeness, explicit expressions of the reduced NN interactions of V_C, V_D, and V_E parts and their partial wave contributions are given in Appendices A and B. Analogous calculations were presented by Holt, Kaiser, and Weise [25]. I, however, do not use an approximation for the off-diagonal

matrix elements assumed there. It is possible to obtain analytical expressions for the partial wave expansion by introducing several functions in a form of the integration of Legendre polynomials of the second kind, as given in Eqs. (B1)–(B6). All terms in V_C and V_D yield central and tensor interactions. Spin-orbit components appear only in the c_1 and c_3 terms of V_C. The V_E interaction gives only an $\ell = 0$ central component; that is, in the $^1S_0$ and $^3S_1$ channels.

Low-energy constants of the Ch-EFT interaction used in numerical calculations in the following sections are those of the Jülich group [8]: $c_1 = -0.81$ GeV^{-1}, $c_3 = -3.4$ GeV^{-1}, and $c_4 = 3.4$ GeV^{-1}. Other constants are taken from the Ref. [18]: $c_D = -4.381$ and $c_E = -1.126$. As noted in Appendix A, reduced effective interaction $V_{12(3)}$ is multiplied by a form factor $\exp\{-(q'/\Lambda)^6 - (q/\Lambda)^6\}$. I adopt the same cutoff Λ as in the NN sector.

It is noted that the parametrization of the Ch-EFT NN interaction in Ref. [8] seems to not yet reach the precision of modern NN potentials even at the N^{3}LO. However, the fit to experimental data in S waves which dominate the contribution to nuclear matter energies is good. The reliable fit, in addition, for other partial waves at lower energies than about 200 MeV is sufficient to perform a quantitative investigation of the nuclear and neutron matter properties. On the basis of such a study, it is worthwhile to examine the contributions of the 3NF which is systematically constructed in the Ch-EFT.

III. NUMERICAL CALCULATIONS IN SYMMETRIC NUCLEAR MATTER

First, we present results of LOBT calculations in symmetric nuclear matter, using only the initial NN part of the Ch-EFT potential. It is expected that the obtained saturation curve is not so dissimilar from those of other modern NN potentials. Ch-EFT potential is regularized by a rather soft form factor as the interaction based on low-energy effective theory. The nuclear-matter energy may depend considerably on the cutoff energy Λ of the regulator. I show, in the beginning, the results of $\Lambda = 550$ MeV, and afterwards discuss the Λ dependence. The obtained saturation curve in symmetric nuclear matter is shown by a dashed curve in Fig. 1, compared to the results of other NN potentials: AV18 [30], NSC [31], and CD-Bonn [32] potentials. It is seen that the saturation curve of the Ch-EFT NN potential is very similar to those of AV18 and NSC. AV18 and NSC potentials have comparatively stronger tensor component than the CD-Bonn potential, which is reflected in the larger deuteron D-state probability. Despite the fact that the Ch-EFT interaction shows a smaller deuteron D-state probability, the LOBT energy is similar to those of AV18 and NSC.

When the effect of the 3NF is included by the procedure explained in Sec. II, I obtain the solid curve shown in Fig. 1. As a basis for comparison, the saturation curve expected from the Gogny force [33], which is a standard effective interaction used for a density-dependent Hartree-Fock description of nuclei, is also plotted. The calculation at higher densities than $k_F = 1.6$ fm^{-1} is unreliable and not shown, because calculated single-particle energies wobble badly at large momentum beyond the normal density where the Ch-EFT as the low-energy

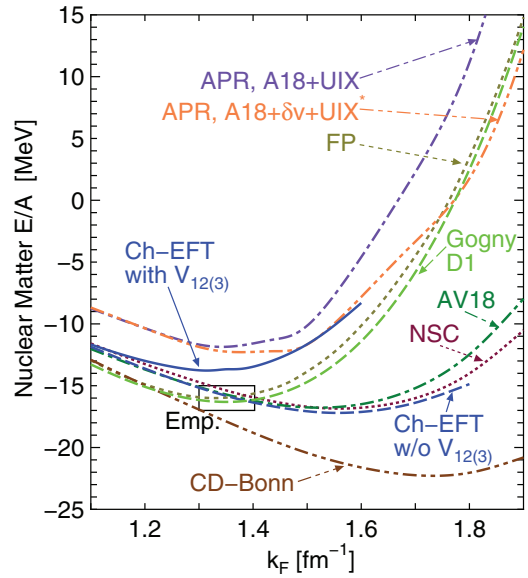

FIG. 1. (Color online) LOBT saturation curves in symmetric nuclear matter, using the Ch-EFT interaction with the cutoff energy of $\Lambda = 550$ MeV. The solid and dashed curves are the results with and without the 3NF effects, respectively. Energies from other modern NN potentials, AV18 [30], NSC [31], and CD-Bonn [32], are also presented. As a basis for comparison, energy expected from the Gogny D1 force [33] is included. In addition, results of variational calculations of the Illinois group with the phenomenological 3NF, FP [15] and APR [16], are included.

theory is not to be applied especially when the reduce NN force is included. The saturation property is much improved by including $V_{12(3)}$, although the energy at the saturation point is shallow by a few MeV. The deviation is probably within the uncertainty of the lowest-order calculation on the one hand, and the uncertainties of low-energy constants as well as the ambiguity of cutoff parameters on the other. Consequently, the longstanding problem of microscopic understanding of the nuclear saturation seems to be resolved by the inclusion of the 3NF. This recognition may not be new, because the role of the 3NF has been demonstrated repeatedly in the literature [14–16]. However, previous calculations inevitably include phenomenological adjustment. The advantage of the present calculation with using the Ch-EFT 3NF interaction is that the potential is systematically constructed and is consistent with the NN sector. The c_3 term of the Ch-EFT 3NF is found to give a dominant repulsive contribution to the energy. This coupling constant is determined in the NN sector and hence no room for an additional adjustment.

To see the contributions of the 3NF in more details, I show, in Fig. 2, partial wave decomposition of the calculated potential energy. The attractive contribution in the $^3S_1$ channel is seen to increase by including the 3NF. This is due to the enhancement of the tensor correlation by the supplemented tensor force. On the other hand, the $^1S_0$ contribution becomes less attractive. The p-wave contributions depend much on the total-angular momentum J. This is owing to the rather strong spin-orbit component. It has been known that the net effect of the triplet p-wave contribution is small, which is a rather

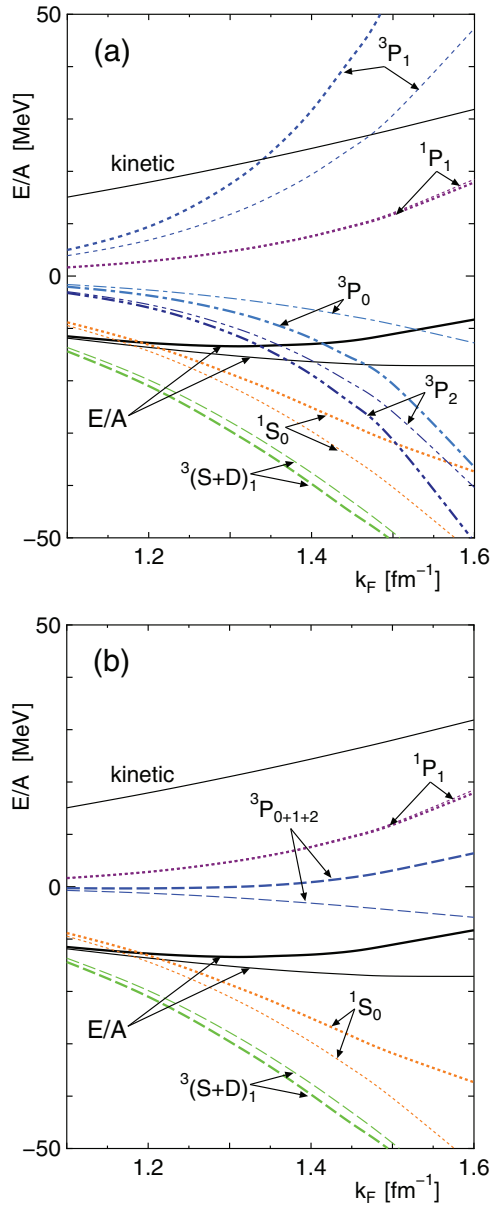

FIG. 2. (Color online) k_F dependence of partial wave contributions to the nuclear-matter LOBT energy per nucleon for the Ch-EFT interaction for $\Lambda = 550$ MeV. Thick and thin curves are with and without the 3NF effects, respectively; (a) full decomposition, (b) different J being summed.

remarkable character of the NN interaction. This property persists after including the 3NF, but the net ^{3}O contribution becomes repulsive when the 3NF is incorporated. The repulsion gradually grows as the density goes up, is important for improving the description of the nuclear saturation property. On the other hand, the singlet p channel is little affected by the 3NF. These characteristics of the 3NF contributions may be used for improving the effective interactions for density-dependent Hartree-Fock calculations and/or density functionals for medium-heavy nuclei.

It has been recognized in nuclear structure calculations that the two-body spin-orbit force is not sufficient to explain a strong single-particle spin-orbit field which is essential to describe empirical nuclear shell structures characterized by nuclear magic numbers. As was indicated in the separate paper [22], the additional spin-orbit strength from the 3NF is favorable to provide the empirical strength of the one-body spin-orbit field. The strength of the nuclear one-body spin-orbit potential from nucleon-nucleon interactions is represented by the Scheerbaum factor $B_S(\bar{q})$, the definition of which is found in Ref. [22]. $B_S(\bar{q})$ corresponds to the spin-orbit strength W of the δ-type two-body spin-orbit interaction $iW(\boldsymbol{\sigma}_1 + \boldsymbol{\sigma}_2) \cdot [\nabla_r \times (\boldsymbol{r})\nabla_r]$ customarily used in nuclear Hartree-Fock calculations. The empirical value of W is around 120 MeV fm^5. Because these results in Ref. [22] were simply obtained by G_{12} and not by $G_{12} + \frac{1}{6}V_{12(3)}(1 + \frac{Q}{\omega - H})G_{12}$ explained in Sec. II, I show revised numbers in Table I. The additional term makes the value of $B_S(\bar{q})$ slightly larger.

TABLE I. Scheerbaum factor $B_S(\bar{q})$ in units of MeV fm^5 with $\bar{q} = 0.7$ fm^{-1} for Jülich N^{3}LO [9] with and without 3NF. The G matrix in Ref. [22] is replaced by $G_{12} + \frac{1}{6}V_{12(3)}(1 + \frac{Q}{\omega - H})G_{12}$ in this calculation.

	Nuclear matter		Neutron matter	
$k_F = 1.35$ fm^{-1}	N^{3}LO	N^{3}LO + 3NF	N^{3}LO	N^{3}LO + 3NF
$B_S(T=0)$	2.5	7.3	–	–
$B_S(T=1)$	84.6	120.2	84.7	93.3
	Nuclear matter		Neutron matter	
$k_F = 1.07$ fm^{-1}	N^{3}LO	N^{3}LO + 3NF	N^{3}LO	N^{3}LO + 3NF
$B_S(T=0)$	1.6	4.4	–	–
$B_S(T=1)$	86.5	109.8	87.0	92.3

Now, I address the cutoff-energy dependence of the calculated LOBT energies. We show, in Fig. 3, saturation curves by using $\Lambda = 450$ MeV and $\Lambda = 600$ MeV, in addition

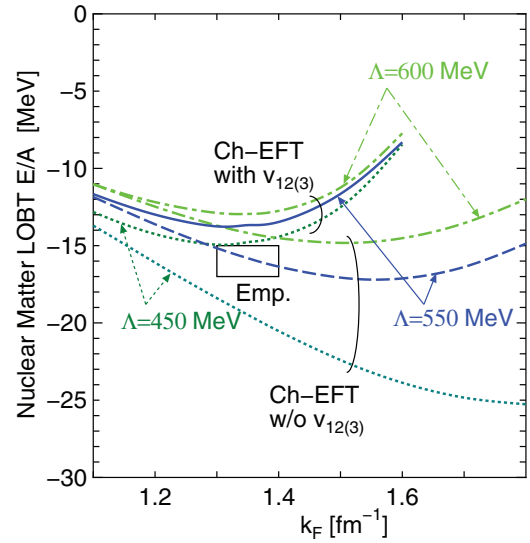

FIG. 3. (Color online) Cutoff Λ dependence of the LOBT energy per nucleon in symmetric nuclear matter for the Ch-EFT interaction with and without the 3NF effects.

to the case of $\Lambda = 550$ MeV presented in Fig. 1. When only the NN interactions of the Ch-EFT are employed, the calculated energies depend considerably on Λ. The smaller cutoff energy provides larger binding energies. The result of $\Lambda = 450$ MeV is rather close to that of the CD-Bonn potential given in Fig. 1. It is impressive to observe that calculated energies with different Λ become very close each other when the 3NF is added. That is, the cutoff-energy dependence is significantly reduced if the NN and 3NF which are constructed consistently in the Ch-EFT are simultaneously used in the LOBT calculation.

It is instructive to examine the cause of the reduction of the Λ dependence by inspecting each spin- and isospin-channel contribution to the potential energy. Table II tabulates the decomposition of the calculated LOBT energies of nuclear matter at $k_F = 1.07$, 1.35, and 1.60 fm^{-1} with and without $V_{12(3)}$ for $\Lambda = 450$, 550, and 600 MeV, respectively. The repulsive effect from $V_{12(3)}$ in the ^{1}O and ^{1}E states depends little on the cutoff Λ. On the other hand, the additional contribution from $V_{12(3)}$ depends on Λ in the channels in which the tensor force exists, namely ^{3}O and ^{3}E. This dependence is thought to be ascribed to the difference of the tensor component. It has been recognized that the NN potential having weaker tensor strength tends to provide larger binding energy, as the saturation curves of the CD-Bonn, Nijmegen, and AV18 potentials in Fig. 1 demonstrate. The saturation curve of the Ch-EFT NN potential with different Λ exhibits this tendency. The smaller Λ means that the pion-exchange tensor part is masked to a larger extent, giving larger binding energy. The additional tensor force in $V_{12(3)}$ tends to provide an attractive effect through the correlation, which explains the reason why the additional contribution becomes attractive in the ^{3}E state and the repulsion in the ^{3}O state decreases with increasing Λ. Such an attraction is smaller for the smaller cutoff-energy Λ as a result of the interplay of the tensor and central components, and therefore the repulsion from the ^{1}E and ^{3}O states raises the saturation curve to reduce the large difference in the NN only case.

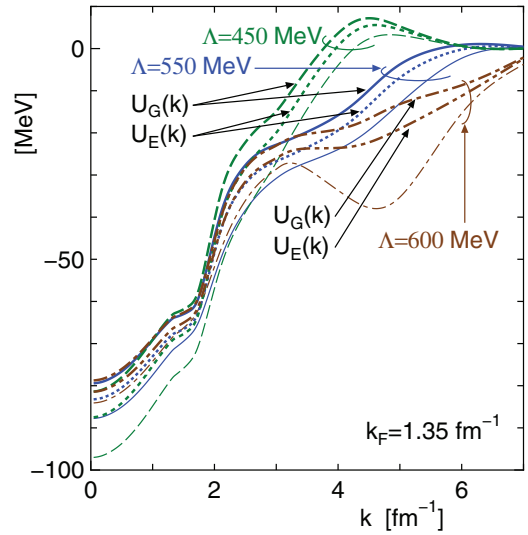

FIG. 4. (Color online) Momentum dependence of single-particle potentials $U_G(k)$, Eq. (6), and $U_E(k)$, Eq. (8), in symmetric nuclear matter for the three instances of the cutoff energy Λ of the Ch-EFT interaction. Thin curves show the results without the 3NF effects.

Finally in this section, I remark on the quantitative difference between $U_G(\boldsymbol{k})$ and $U_E(\boldsymbol{k})$ defined in Eqs. (6) and (8), respectively. Figure 4 compares $U_G(\boldsymbol{k})$ and $U_E(\boldsymbol{k})$ with the NN force and 3NF for three instances of the cutoff energy Λ. The single-particle potential $U_E(\boldsymbol{k})$ without the 3NF effects is also shown. The difference of $U_G(\boldsymbol{k})$ and $U_E(\boldsymbol{k})$, which

TABLE II. Total energies and spin- and isospin-channel (^{1}O, ^{3}E, ^{1}E, and ^{3}O) decompositions for three instances of the cutoff energy Λ (MeV) at $k_F = 1.07$, 1.35, and 1.60 fm^{-1} for symmetric nuclear matter, and at $k_F = 1.35$ and 1.80 fm^{-1} for pure neutron matter. The corresponding density ρ (fm^{-3}), kinetic energy T, and total potential energy contribution U are also tabulated. Energies are in units of MeV.

			Symmetric nuclear matter without 3NF							Symmetric nuclear matter with 3NF					
k_F	ρ	Λ	E/A	T	U	^{1}O	^{3}E	^{1}E	^{3}O	E/A	U	^{1}O	^{3}E	^{1}E	^{3}O
1.07	0.083	450	–13.01	14.24	–27.25	1.98	–17.61	–11.13	–0.50	–12.31	–26.55	1.94	–17.96	–10.43	–0.10
		550	–11.32	14.24	–25.56	1.99	–16.17	–10.95	–0.43	–11.21	–25.45	1.95	–17.04	–10.26	–0.11
		600	–10.57	14.24	–24.81	2.04	–15.38	–11.03	–0.43	–10.62	–24.87	2.00	–16.39	–10.35	–0.13
1.35	0.166	450	–19.47	22.67	–42.15	4.67	–27.38	–18.28	–1.16	–14.77	–37.45	4.43	–27.21	–15.50	0.84
		550	–15.81	22.67	–38.49	4.74	–24.10	–18.25	–0.88	–13.67	–36.34	4.49	–25.86	–15.59	0.60
		600	–14.18	22.67	–36.85	4.85	–22.26	–18.60	–0.84	–12.95	–35.62	4.60	–24.73	–15.97	0.48
1.60	0.277	450	–23.87	31.85	–55.72	8.67	–37.55	–25.36	–1.48	–8.45	–40.30	7.84	–35.07	–17.89	4.82
		550	–17.12	31.85	–48.97	9.00	–31.22	–25.85	–0.89	–8.31	–40.16	8.10	–33.28	–18.19	3.21
		600	–14.52	31.85	–46.37	9.13	–27.75	–26.99	–0.75	–7.73	–39.58	8.24	–31.02	–19.19	2.39
			Pure neutron matter without 3NF							Pure neutron matter with 3NF					
1.35	0.083	450	8.25	22.67	–14.43	0.0	0.0	–13.52	–0.91	9.29	–13.38	0.0	0.0	–13.12	–0.26
		550	8.21	22.67	–14.46	0.0	0.0	–13.69	–0.78	9.08	–13.60	0.0	0.0	–13.34	–0.26
		600	8.24	22.67	–14.43	0.0	0.0	–13.68	–0.75	9.09	–13.58	0.0	0.0	–13.32	–0.27
1.80	0.197	450	17.04	40.31	–23.27	0.0	0.0	–22.49	–0.78	24.66	–15.65	0.0	0.0	–19.75	4.09
		550	15.75	40.31	–24.56	0.0	0.0	–24.03	–0.53	21.45	–18.86	0.0	0.0	–22.19	3.33
		600	14.69	40.31	–25.62	0.0	0.0	–25.32	–0.30	20.33	–19.98	0.0	0.0	–22.99	3.01

is $\sum_{k'} \frac{1}{6}\langle \boldsymbol{k}\boldsymbol{k}' V_{12(3)}(1+\frac{Q}{\omega-H})G_{12}|\boldsymbol{k}\boldsymbol{k}'\rangle_A$, is on the order of 5 MeV for $|\boldsymbol{k}| \leqslant 2$ fm^{-1}. That is, the single-particle energy is raised by around 5 MeV by the additional term. Through the starting energy dependence of the G matrix, the total energy per nucleon is lowered by about 0.5 MeV. The large Λ dependence of the single-particle potential beyond $|\boldsymbol{k}| = 3$ fm^{-1} has no physical significance. As the results in Fig. 3 suggest, $U_E(\boldsymbol{k})$ for $|\boldsymbol{k}| \lesssim 2$ fm^{-1} does not depend much on the cutoff energy, when the 3NF is included.

IV. NUMERICAL CALCULATIONS IN PURE NEUTRON MATTER

The energy per nucleon of neutron matter is fundamental to determine properties of neutron star matter. The k_F dependence of the calculated LOBT energies in pure neutron matter with and without including the 3NF is shown in Fig. 5. Energies obtained with other modern NN potentials and results of the variational calculation by the Illinois group [15,16] are also presented for comparison. The latter used the AV18 potential [30] and included the 3NF of the Fujita-Miyazawa [11] type supplemented by phenomenological terms. Because the strong tensor effect in the $^3S_0$-$^3D_0$ channel is absent, many-body correlations are relatively simple in neutron matter. Since the calculated saturation curve in symmetric nuclear matter already well corresponds to the empirical one, present LOBT energy in neutron matter is expected to be trustful. In contrast to symmetric nuclear matter, calculated energies with different NN potentials are very similar, as is seen in the k_F dependence of neutron matter energies with Ch-EFT, AV18, NSC, and CD-Bonn potentials in Fig. 5.

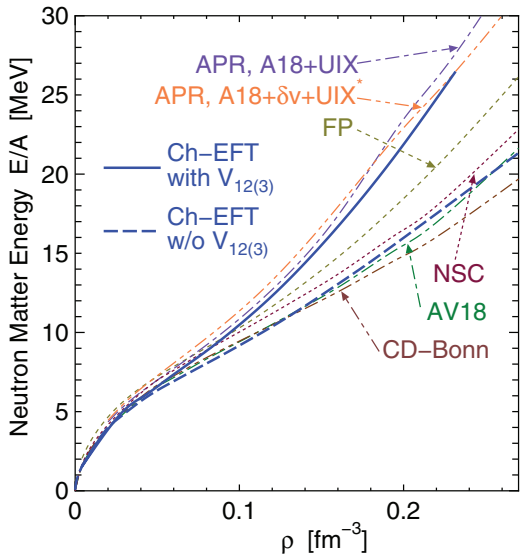

FIG. 5. (Color online) Calculated LOBT energy per nucleon in pure neutron matter, utilizing the Ch-EFT interaction with the cutoff energy of $\Lambda = 550$ MeV with and without including the effects of the 3NF. Energies from other modern NN potentials, AV18 [30], NSC [31], and CD-Bonn [32], and results of variational calculations of the Illinois group, FP [15] and APR [16], are also shown.

The Ch-EFT 3NF itself is more predictive for the application to neutron matter, because the contact c_E term vanishes in pure neutron matter as the Pauli principle forbids three neutrons to assemble at the same place, and the c_D term which gives null in the plane wave case gives a negligibly small contribution. In addition, the c_4 term does not contribute. Thus the contribution from the NNLO 3NF is determined by the c_1 and c_3 terms. These coupling constants are determined in the NN sector.

The results of the variational calculation in Ref. [16] shown in Fig. 5 have been utilized as the canonical equation of state (EoS) for discussing neutron star matter properties. It is interesting to realize that the LOBT result obtained by including the 3NF, in which no phenomenological adjustment is introduced, is close to the EoS of Ref. [16].

As the Ch-EFT cannot be applied to the high momentum region, it is not possible to discuss directly the EoS relevant to the core of high-density neutron stars. Nevertheless, it is possible to provide the reference EoS at lower densities which should be smoothly matched to the EoS obtained by theories designed for the high density region. Such an effort was recently reported in Ref. [34].

As noted in Ref. [22], the magnitude of the spin-orbit component in $V_{12(3)}$ obtained in pure neutron matter is one third of that in symmetric nuclear matter. Although correlations somewhat modify this number, as is given in Table I, the calculated additional contribution to the Scheerbaum factor from the 3NF in neutron matter is about one-third of that in nuclear matter. Observing that the contribution of the genuine NN interaction to the single-particle spin-orbit strength is insensitive to the neutron-proton asymmetry $\alpha = \frac{N-Z}{N+Z}$, the 3NF can be the source of the asymmetry dependence of the strength of the single-particle spin-orbit potential. In a Woods-Saxon potential model, rather strong α dependence, such as $(1 - 0.54\alpha)$ was inferred, as in the textbook by

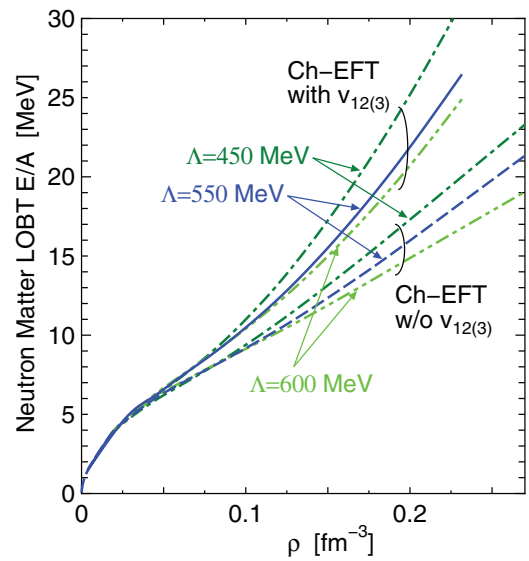

FIG. 6. (Color online) Cutoff Λ dependence of the LOBT energy per nucleon in pure neutron matter for the Ch-EFT interaction with and without the 3NF effects.

Bohr-Mottelson [35]. Recent fitting by Wyss suggests gentler α dependence, typically $1 - 0.25\alpha$ as is given in Table I of Ref. [36]. If I naively use the calculated numbers given in Table I and assume that $B_S(T = 1)$ in neutron matter depends little on the density, the α dependence of the single-particle spin-orbit strength is estimated as $(1 - 0.22\alpha)$, which is consistent with the value mentioned above.

Finally, Fig. 6 shows the variation in the neutron-matter energy for a different choice of the cutoff energy Λ. Explicit values of the ^{1}E and ^{3}O contributions to the energy are given in Table II at $k_F = 1.35$ and 1.8 fm^{-1}, which correspond to $\rho = 0.083$ and 0.2 fm^{-3}, respectively. ^{3}E state being absent, the cutoff-energy dependence is already moderate in the case of the NN interaction only. Although the ^{3}O repulsion becomes smaller with growing Λ, this does not work to reduce the Λ dependence when including $V_{12(3)}$.

V. SUMMARY

We have calculated LOBT energies both in symmetric nuclear matter and pure neutron matter, using the Ch-EFT N^{3}LO NN interaction and NNLO 3NF of the Jülich group [8]. In the Ch-EFT, the 3NF is introduced in a systematic way along with the NN potential. Three of the five coupling constants in the NNLO 3NF are fixed in a NN sector. The remaining two parameters are under control in the literature in terms of reproducing the properties of few-nucleon systems. The 3NF is treated by reducing it to density-dependent NN interactions by folding single-nucleon degrees of freedom in infinite matter. We have given, in the Appendices, explicit expressions of the reduced NN interactions and their partial-wave expanded forms.

Calculated results show that the empirical saturation property is well reproduced in nuclear matter. In a conventional understanding, the effects of Pauli blocking for the strong tensor coupling have been emphasized as the basic mechanism of bringing about nuclear saturation. Though this effect is fundamentally important, the sizable repulsive contribution of the 3NF is also crucial in the region around and above normal nuclear matter density. This indicates that Pauli blocking not only for the standard tensor correlation but also for other non-nucleonic excitations inherent in the two-nucleon process, such as Δ isobar and antinucleon excitations, provides large repulsive effects.

It is noteworthy that the large cutoff-energy dependence of the calculated energies obtained only with the Ch-EFT NN force is reduced substantially when including the 3NF effects. This dependence arises predominantly in the triplet even channel; that is, the channel in which the tensor correlation is significant. Therefore, the cutoff-energy dependence is weak in neutron matter.

The contributions of the 3NF in the ^{1}E and ^{3}O channels are repulsive. Owing to the repulsion, the density dependence of neutron matter energy per nucleon becomes very close to those favorable for describing neutron star properties, although the prediction of Ch-EFT cannot be applied at high densities. The strength of the spin-orbit component in the ^{3}O channel increases by about 30%, which resolves the problem of the insufficiency of modern NN potentials to account for the empirical spin-orbit strength, as previously reported in Ref. [22]. The potential energy in the $^3S_1$ state turns out to be more attractive due to the enhancement of the tensor component. The knowledge of these specific properties of the 3NF contributions may be helpful for improving effective forces and/or energy functionals for finite nuclei.

I conclude that although more rigorous treatment of the 3NF together with more than three-body correlations are required in the future, the present calculations demonstrate that the 3NF constructed in a consistent way with the NN part in the sense of effective field theory can reproduce basic nuclear properties, namely the saturation and strong spin-orbit field, without phenomenological adjustments.

ACKNOWLEDGMENTS

This work is supported by JSPS KAKENHI Grant Nos. 22540288 and 25400266. The author thanks H. Kamada for valuable comments concerning the Ch-EFT interactions. He is also grateful to M. Yahiro and Y. R. Shimizu for their interest in this work.

APPENDIX A: EFFECTIVE NN FORCES FROM THE 3NF IN CHIRAL EFFECTIVE FIELD THEORY

In the leading order, NNLO, three-nucleon force V_{123} consists of terms specified by five low-energy coupling constants c_1, c_3, c_4, c_D, and c_E: $V_{123} = V_C + V_D + V_E$. Each term is given as follows:

$$V_C = \frac{1}{2}\left(\frac{g_A}{2f_\pi}\right)^2 \sum_{i\neq j\neq k} \frac{(\boldsymbol{\sigma}_i\cdot\boldsymbol{q}_i)(\boldsymbol{\sigma}_j\cdot\boldsymbol{q}_j)}{(q_i^2+m_\pi^2)(q_j^2+m_\pi^2)}\tau_i^\alpha\tau_j^\beta \times\left\{\delta^{\alpha\beta}\left[-\frac{4c_1m_\pi^2}{f_\pi^2}+\frac{2c_3}{f_\pi^2}\boldsymbol{q}_i\cdot\boldsymbol{q}_j\right] +\sum_\gamma\frac{c_4}{f_\pi^2}\epsilon^{\alpha\beta\gamma}\tau_k^\gamma\boldsymbol{\sigma}_k\cdot(\boldsymbol{q}_i\times\boldsymbol{q}_j)\right\}, \tag{A1}$$

$$V_D = -\frac{g_A}{8f_\pi^2}\frac{c_D}{f_\pi^2\Lambda_\chi}\sum_{i\neq j\neq k}\frac{(\boldsymbol{\sigma}_j\cdot\boldsymbol{q}_j)(\boldsymbol{\sigma}_i\cdot\boldsymbol{q}_j)}{q_j^2+m_\pi^2}(\boldsymbol{\tau}_i\cdot\boldsymbol{\tau}_j), \tag{A2}$$

$$V_E = \frac{c_E}{2f_\pi^4\Lambda_\chi}\sum_{j\neq k}(\boldsymbol{\tau}_j\cdot\boldsymbol{\tau}_k) = \frac{c_E}{f_\pi^4\Lambda_\chi}(\boldsymbol{\tau}_1\cdot\boldsymbol{\tau}_2+\boldsymbol{\tau}_2\cdot\boldsymbol{\tau}_3+\boldsymbol{\tau}_3\cdot\boldsymbol{\tau}_1). \tag{A3}$$

Three coupling constants c_1, c_3, and c_3 are determined in the NN sector and the remaining c_D and c_E are adjusted in more than three nucleon systems. As is explained in Eq. (1), the three-nucleon force V_{123} is reduced to an effective NN force $V_{12(3)}$ by summing over the third nucleon in the Fermi sea:

$$\langle\boldsymbol{k}_1'\sigma_1'\tau_1', -\boldsymbol{k}_1'\sigma_2'\tau_2'|V_{12(3)}|\boldsymbol{k}_1\sigma_1\tau_1,-\boldsymbol{k}_1\sigma_2\tau_2\rangle_a \equiv \sum_{\boldsymbol{k}_3,\sigma_3\tau_3}\langle\boldsymbol{k}_1'\sigma_1'\tau_1',-\boldsymbol{k}_1'\sigma_2'\tau_2',\boldsymbol{k}_3\sigma_3\tau_3| \times V_{123}|\boldsymbol{k}_1\sigma_1\tau_1,-\boldsymbol{k}_1\sigma_2\tau_2,\boldsymbol{k}_3\sigma_3\tau_3\rangle_a. \tag{A4}$$

Form factors are not taken into account in this folding procedure. The obtained $V_{12(3)}$ is multiplied by a form factor in the form of $\exp\{-(q'/\Lambda)^6 - (q/\Lambda)^6\}$.

In this appendix, I present details of the matrix elements of $\langle \boldsymbol{k}'_1\sigma'_1\tau'_1, -\boldsymbol{k}'_1\sigma'_2\tau'_2|V_{12(3)}|\boldsymbol{k}_1\sigma_1\tau_1, -\boldsymbol{k}_1\sigma_2\tau_2\rangle$ from Ch-EFT 3NF forces V_C, V_D, and V_E. In the following, I use the standard notation for the tensor operator $S_{12}(\boldsymbol{k}',\boldsymbol{k})$ and their matrix elements between partial waves:

$$S_{12}(\boldsymbol{k}',\boldsymbol{k}) = 3([\boldsymbol{\sigma}_1\times\boldsymbol{\sigma}_2]^2\cdot[\boldsymbol{k}'\times\boldsymbol{k}]^2), \tag{A5}$$

$$(S_{12})^{\ell'}_{\ell 1J} = \frac{6\sqrt{J(J+1)}}{2J+1} \quad \text{for} \quad \ell' = \ell+2 \quad \text{or} \quad \ell' = \ell-2, \tag{A6}$$

$$(S_{12})^{J}_{J1J} = 2, \quad (S_{12})^{J+1}_{J+11J} = -\frac{2(J+2)}{2J+1}, \quad \text{and} \quad (S_{12})^{J-1}_{J-11J} = -\frac{2(J-1)}{2J+1}. \tag{A7}$$

Evaluating Eq. (A4), the c_1 term of V_C provides

$$\begin{aligned}
&\frac{c_1 g_A^2 m_\pi^2 \rho_0}{f_\pi^4}\frac{(\boldsymbol{\sigma}_1\cdot(\boldsymbol{k}'_1-\boldsymbol{k}_1))(\boldsymbol{\sigma}_2\cdot(\boldsymbol{k}'_1-\boldsymbol{k}_1))}{\big((\boldsymbol{k}'_1-\boldsymbol{k}_1)^2+m_\pi^2\big)\big((\boldsymbol{k}'_1-\boldsymbol{k}_1)^2+m_\pi^2\big)}(\boldsymbol{\tau}_1\cdot\boldsymbol{\tau}_2)\\
&+\frac{c_1 g_A^2 m_\pi^2}{f_\pi^4}\sum_{\boldsymbol{k}_3}\Bigg(\frac{\frac{2}{3}(\boldsymbol{\sigma}_1\cdot\boldsymbol{\sigma}_2)(\boldsymbol{k}'_1-\boldsymbol{k}_1)\cdot(\boldsymbol{k}_3+\boldsymbol{k}_1)+2([\boldsymbol{\sigma}_1\times\boldsymbol{\sigma}_2]^2\cdot[(\boldsymbol{k}'_1-\boldsymbol{k}_1)\times(\boldsymbol{k}_3+\boldsymbol{k}_1)]^2)}{\big((\boldsymbol{k}'_1-\boldsymbol{k}_1)^2+m_\pi^2\big)\big((\boldsymbol{k}_3+\boldsymbol{k}_1)^2+m_\pi^2\big)}\\
&+\frac{\frac{2}{3}(\boldsymbol{\sigma}_1\cdot\boldsymbol{\sigma}_2)(\boldsymbol{k}'_1-\boldsymbol{k}_3)\cdot(\boldsymbol{k}_1-\boldsymbol{k}'_1)+2([\boldsymbol{\sigma}_1\times\boldsymbol{\sigma}_2]^2\cdot[(\boldsymbol{k}'_1-\boldsymbol{k}_3)\times(\boldsymbol{k}_1-\boldsymbol{k}'_1)]^2)}{\big((\boldsymbol{k}'_1-\boldsymbol{k}_3)^2+m_\pi^2\big)\big((\boldsymbol{k}'_1-\boldsymbol{k}_1)^2+m_\pi^2\big)}\Bigg)(\boldsymbol{\tau}_1\cdot\boldsymbol{\tau}_2)\\
&+\frac{c_1 g_A^2 m_\pi^2}{f_\pi^4}\sum_{\boldsymbol{k}_3}\frac{6(\boldsymbol{k}'_1-\boldsymbol{k}_3)\cdot(\boldsymbol{k}_3-\boldsymbol{k}_1)+3i(\boldsymbol{\sigma}_1+\boldsymbol{\sigma}_2)\cdot\big((\boldsymbol{k}'_1-\boldsymbol{k}_3)\times(\boldsymbol{k}_3-\boldsymbol{k}_1)\big)}{\big((\boldsymbol{k}'_1-\boldsymbol{k}_3)^2+m_\pi^2\big)((\boldsymbol{k}_3-\boldsymbol{k}_1)^2+m_\pi^2)},
\end{aligned} \tag{A8}$$

the c_3 term of V_C

$$\begin{aligned}
&\frac{c_3 g_A^2\rho_0}{2f_\pi^4}\frac{(\boldsymbol{\sigma}_1\cdot(\boldsymbol{k}'_1-\boldsymbol{k}_1))(\boldsymbol{\sigma}_2\cdot(\boldsymbol{k}'_1-\boldsymbol{k}_1))}{\big((\boldsymbol{k}'_1-\boldsymbol{k}_1)^2+m_\pi^2\big)^2}|\boldsymbol{k}'_1-\boldsymbol{k}_1|^2(\boldsymbol{\tau}_1\cdot\boldsymbol{\tau}_2)-\frac{c_3 g_A^2}{2f_\pi^4}\frac{\frac{2}{3}(\boldsymbol{\tau}_1\cdot\boldsymbol{\tau}_2)(\boldsymbol{\sigma}_1\cdot\boldsymbol{\sigma}_2)}{(\boldsymbol{k}'_1-\boldsymbol{k}_1)^2+m_\pi^2}\Bigg\{((\boldsymbol{k}'_1-\boldsymbol{k}_1)\cdot\boldsymbol{k}_1)^2(F_0(k_1)-2F_1(k_1))\\
&+((\boldsymbol{k}'_1-\boldsymbol{k}_1)\cdot\boldsymbol{k}'_1)^2(F_0(k'_1)-2F_1(k'_1))+\frac{1}{3}|\boldsymbol{k}'_1-\boldsymbol{k}_1|^2\big(k_1^2F_2(k_1)+k_1'^2F_2(k'_1)\big)\\
&+\frac{1}{k_1^2}([(\boldsymbol{k}'_1-\boldsymbol{k}_1)\times(\boldsymbol{k}'_1-\boldsymbol{k}_1)]^2\cdot[\boldsymbol{k}_1\times\boldsymbol{k}_1]^2)k_1^2F_3(k_1)+\frac{1}{k_1^2}([(\boldsymbol{k}'_1-\boldsymbol{k}_1)\times(\boldsymbol{k}'_1-\boldsymbol{k}_1)]^2\cdot[\boldsymbol{k}'_1\times\boldsymbol{k}'_1]^2)k_1'^2F_3(k'_1)\Bigg\}\\
&+\frac{c_3 g_A^2}{2f_\pi^4}\frac{2(\boldsymbol{\tau}_1\cdot\boldsymbol{\tau}_2)}{(\boldsymbol{k}'_1-\boldsymbol{k}_1)^2+m_\pi^2}\Bigg\{\frac{1}{3}S_{12}(\boldsymbol{k}'_1-\boldsymbol{k}_1,\boldsymbol{k}_1)((\boldsymbol{k}'_1-\boldsymbol{k}_1)\cdot\boldsymbol{k}_1)(F_0(k_1)-2F_1(k_1))\\
&+\frac{1}{3}S_{12}(\boldsymbol{k}'_1-\boldsymbol{k}_1,\boldsymbol{k}'_1)((\boldsymbol{k}'_1-\boldsymbol{k}_1)\cdot\boldsymbol{k}'_1)(F_0(k'_1)-2F_1(k'_1))+\frac{1}{9}S_{12}(\boldsymbol{k}'_1-\boldsymbol{k}_1,\boldsymbol{k}'_1-\boldsymbol{k}_1)\big(k_1^2F_2(k_1)+k_1'^2F_2(k'_1)\big)\\
&-\frac{1}{9}\big[S_{12}(\boldsymbol{k}_1,\boldsymbol{k}_1)\big(-2k_1^2+3(\boldsymbol{k}_1\cdot\boldsymbol{k}'_1)\big)+S_{12}(\boldsymbol{k}'_1,\boldsymbol{k}'_1)k_1^2+S_{12}(\boldsymbol{k}'_1,\boldsymbol{k}_1)\big(k_1^2-3(\boldsymbol{k}_1\cdot\boldsymbol{k}'_1)\big)\big]F_3(k_1)\\
&-\frac{1}{9}\big[S_{12}(\boldsymbol{k}'_1,\boldsymbol{k}'_1)\big(-2k_1'^2+3(\boldsymbol{k}_1\cdot\boldsymbol{k}'_1)\big)+S_{12}(\boldsymbol{k}_1,\boldsymbol{k}_1)k_1'^2+S_{12}(\boldsymbol{k}'_1,\boldsymbol{k}_1)\big(k_1'^2-3(\boldsymbol{k}_1\cdot\boldsymbol{k}'_1)\big)\big]F_3(k'_1)\Bigg\}\\
&+\frac{c_3 g_A^2}{2f_\pi^4}\sum_{\boldsymbol{k}_3}\frac{6(\boldsymbol{k}'_1-\boldsymbol{k}_3)\cdot(\boldsymbol{k}_3-\boldsymbol{k}_1)+3i(\boldsymbol{\sigma}_1+\boldsymbol{\sigma}_2)\cdot((\boldsymbol{k}'_1-\boldsymbol{k}_1)\times\boldsymbol{k}_3-\boldsymbol{k}'_1\times\boldsymbol{k}_1)}{\big((\boldsymbol{k}'_1-\boldsymbol{k}_3)^2+m_\pi^2\big)\big((\boldsymbol{k}_3-\boldsymbol{k}_1)^2+m_\pi^2\big)}(\boldsymbol{k}'_1-\boldsymbol{k}_3)\cdot(\boldsymbol{k}_3-\boldsymbol{k}_1),
\end{aligned} \tag{A9}$$

and the c_4 term of V_C

$$\begin{aligned}
&2\frac{c_4 g_A^2}{4f_\pi^4}\sum_{\boldsymbol{k}_3}\Bigg\{\frac{(\boldsymbol{\sigma}_1\cdot(\boldsymbol{k}'_1-\boldsymbol{k}_1))(\boldsymbol{\sigma}_2\cdot((-\boldsymbol{k}'_1-\boldsymbol{k}_3)\times((\boldsymbol{k}'_1-\boldsymbol{k}_1)\times(-\boldsymbol{k}'_1-\boldsymbol{k}_3))))}{\big((\boldsymbol{k}'_1-\boldsymbol{k}_1)^2+m_\pi^2\big)\big((-\boldsymbol{k}'_1-\boldsymbol{k}_3)^2+m_\pi^2\big)}\\
&+\frac{(\boldsymbol{\sigma}_1\cdot(\boldsymbol{k}'_1-\boldsymbol{k}_1))(\boldsymbol{\sigma}_2\cdot(((\boldsymbol{k}_3+\boldsymbol{k}_1)\times(\boldsymbol{k}'_1-\boldsymbol{k}_1))\times(\boldsymbol{k}_3+\boldsymbol{k}_1)))}{\big((\boldsymbol{k}'_1-\boldsymbol{k}_1)^2+m_\pi^2\big)\big((\boldsymbol{k}_3+\boldsymbol{k}_1)^2+m_\pi^2\big)}\\
&+\frac{(\boldsymbol{\sigma}_1\cdot((\boldsymbol{k}'_1-\boldsymbol{k}_3)\times(\boldsymbol{k}_1-\boldsymbol{k}_3)))(\boldsymbol{\sigma}_2\cdot((\boldsymbol{k}'_1-\boldsymbol{k}_3)\times(\boldsymbol{k}_1-\boldsymbol{k}_3)))}{\big((\boldsymbol{k}'_1-\boldsymbol{k}_3)^2+m_\pi^2\big)\big((\boldsymbol{k}_1-\boldsymbol{k}_3)^2+m_\pi^2\big)}
\end{aligned}$$

$$
\begin{aligned}
&- \frac{(\boldsymbol{\sigma}_1 \cdot ((\boldsymbol{k}_1' - \boldsymbol{k}_3) \times ((\boldsymbol{k}_1' - \boldsymbol{k}_3) \times (-\boldsymbol{k}_1' + \boldsymbol{k}_1))))(\boldsymbol{\sigma}_2 \cdot (-\boldsymbol{k}_1' + \boldsymbol{k}_1))}{\big((\boldsymbol{k}_1' - \boldsymbol{k}_3)^2 + m_\pi^2\big)\big((\boldsymbol{k}_1' - \boldsymbol{k}_1)^2 + m_\pi^2\big)} \\
&- \frac{(\boldsymbol{\sigma}_1 \cdot ((\boldsymbol{k}_1' - \boldsymbol{k}_3) \times (\boldsymbol{k}_3 - \boldsymbol{k}_1)))(\boldsymbol{\sigma}_2 \cdot (\boldsymbol{k}_3 - \boldsymbol{k}_1) \times (\boldsymbol{k}_1' - \boldsymbol{k}_3))}{\big((\boldsymbol{k}_1' - \boldsymbol{k}_3)^2 + m_\pi^2\big)\big((\boldsymbol{k}_3 - \boldsymbol{k}_1)^2 + m_\pi^2\big)} \\
&- \frac{(\boldsymbol{\sigma}_1 \cdot (((-\boldsymbol{k}_1' + \boldsymbol{k}_1) \times (\boldsymbol{k}_3 - \boldsymbol{k}_1)) \times (\boldsymbol{k}_3 - \boldsymbol{k}_1)))(\boldsymbol{\sigma}_2 \cdot (-\boldsymbol{k}_1' + \boldsymbol{k}_1))}{\big((-\boldsymbol{k}_1' + \boldsymbol{k}_1)^2 + m_\pi^2\big)\big((\boldsymbol{k}_3 - \boldsymbol{k}_1)^2 + m_\pi^2\big)} \Bigg\} (\boldsymbol{\tau}_1 \cdot \boldsymbol{\tau}_2). \qquad \text{(A10)}
\end{aligned}
$$

The V_D term is found to yield

$$
\begin{aligned}
&- \frac{g_A}{8f_\pi^2} \frac{c_D \rho_0}{f_\pi^2 \Lambda_\chi} \frac{\frac{1}{3}(\boldsymbol{\sigma}_1 \cdot \boldsymbol{\sigma}_2)(\boldsymbol{k}_1' - \boldsymbol{k}_1)^2 + ([\boldsymbol{\sigma}_1 \times \boldsymbol{\sigma}_2]^2 \cdot [(\boldsymbol{k}_1' - \boldsymbol{k}_1) \times (\boldsymbol{k}_1' - \boldsymbol{k}_1)]^2)}{(\boldsymbol{k}_1' - \boldsymbol{k}_1)^2 + m_\pi^2} (\boldsymbol{\tau}_1 \cdot \boldsymbol{\tau}_2) \\
&+ 2 \frac{g_A}{8f_\pi^2} \frac{c_D}{f_\pi^2 \Lambda_\chi} \Bigg\{ \frac{1}{3}(\boldsymbol{\sigma}_1 \cdot \boldsymbol{\sigma}_2) \bigg(\frac{1}{2}\rho_0 - m_\pi^2 F_0(k_1) - m_\pi^2 F_0(k_1') \bigg) + ([\boldsymbol{\sigma}_1 \times \boldsymbol{\sigma}_2]^2 \cdot [(\boldsymbol{k}_1' - \boldsymbol{k}_1) \times (\boldsymbol{k}_1' - \boldsymbol{k}_1)]^2)(F_0(k_1) - 2F_1(k_1) \\
&+ F_3(k_1) + F_0(k_1') - 2F_1(k_1') + F_3(k_1')) \Bigg\} (\boldsymbol{\tau}_1 \cdot \boldsymbol{\tau}_2) + 6 \frac{g_A}{8f_\pi^2} \frac{c_D}{f_\pi^2 \Lambda_\chi} \bigg\{ \frac{1}{2}\rho_0 - m_\pi^2 F_0(k_1) - m_\pi^2 F_0(k_1') \bigg\}. \qquad \text{(A11)}
\end{aligned}
$$

Finally, the V_E term gives a spin- and isospin-scalar interaction:

$$
-6 \frac{C_E \frac{1}{4}\rho_0}{f_\pi^4 \Lambda_\chi}. \qquad \text{(A12)}
$$

In the above expressions, Eqs. (A9) and (A11), functions F_0, F_1, F_2, and F_4 are defined as follows:

$$
\begin{aligned}
F_0(k) &\equiv \frac{1}{(2\pi)^3} \iiint_{|\boldsymbol{k}'| \leqslant k_F} d\boldsymbol{k}' \frac{1}{(\boldsymbol{k} - \boldsymbol{k}')^2 + m_\pi^2} \\
&= \frac{1}{(2\pi)^2} \Bigg\{ k_F + \frac{k_F^2 + m_\pi^2 - k^2}{4k} \log \frac{(k + k')^2 + m_\pi^2}{(k - k')^2 + m_\pi^2} - m_\pi \bigg(\arctan \frac{k + k_F}{m_\pi} - \arctan \frac{k - k_F}{m_\pi} \bigg) \Bigg\}, \qquad \text{(A13)} \\
F_1(k) &\equiv \frac{1}{k} \frac{1}{(2\pi)^3} \iiint_{|\boldsymbol{k}'| \leqslant k_F} d\boldsymbol{k}' \frac{k' \cos\theta}{(\boldsymbol{k} - \boldsymbol{k}')^2 + m_\pi^2} \\
&= \frac{1}{k} \frac{1}{(2\pi)^2} \Bigg[\frac{k_F}{4k} \big(3k^2 - k_F^2 - m_\pi^2\big) - k m_\pi \bigg(\arctan \frac{k + k_F}{m_\pi} - \arctan \frac{k - k_F}{m_\pi} \bigg) \\
&\quad + \frac{1}{16k^2} \big\{ m_\pi^4 + 2m_\pi^2 \big(3k^2 + k_F^2\big) + \big(k_F^2 - k^2\big)\big(k_F^2 + 3k^2\big) \big\} \log \frac{(k + k_F)^2 + m_\pi^2}{(k - k_F)^2 + m_\pi^2} \Bigg], \qquad \text{(A14)} \\
F_2(k) &\equiv \frac{2\pi}{(2\pi)^3} \frac{1}{k^3} \int_0^{k_F} dk' k'^3 Q_0 \bigg(\frac{k^2 + k'^2 + m_\pi^2}{2kk'} \bigg) \\
&= \frac{1}{(2\pi)^2} \frac{1}{k^2} \Bigg\{ \frac{1}{6} k_F \big(3k^2 + k_F^2 - 9m_\pi^2\big) + \frac{\big(k_F^4 - k^4 - m_\pi^4 + 6k^2 m_\pi^2\big)}{8k} \log \frac{(k + k_F)^2 + m_\pi^2}{(k - k_F)^2 + m_\pi^2} \\
&\quad + m_\pi \big(m_\pi^2 - k^2\big) \bigg(\arctan \frac{k + k_F}{m_\pi} - \arctan \frac{k - k_F}{m_\pi} \bigg) \Bigg\}, \qquad \text{(A15)} \\
F_3(k) &\equiv \frac{2\pi}{(2\pi)^3} \frac{1}{k^3} \int_0^{k_F} dk' k'^3 Q_2 \bigg(\frac{k^2 + k'^2 + m_\pi^2}{2kk'} \bigg) \\
&= \frac{1}{k^2} \frac{1}{(2\pi)^2} \Bigg\{ \frac{1}{32k^3} \big[\big(k_F^2 + k^2 + m_\pi^2\big)^3 + 2k^2 m_\pi^2 \big(m_\pi^2 + 6k^2\big) - 2k^2 \big(k_F^4 + 3k^4\big) \big] \log \frac{(k + k_F)^2 + m_\pi^2}{(k - k_F)^2 + m_\pi^2} \\
&\quad - k^2 m_\pi \bigg(\arctan \frac{k + k_F}{m_\pi} - \arctan \frac{k - k_F}{m_\pi} \bigg) - \frac{k_F}{8k^2} \bigg(m_\pi^4 + 4k^2 m_\pi^2 + k_F^4 - 5k^4 + \frac{4}{3} k^2 k_F^2 + 2m_\pi^2 k_F^2 \bigg) \Bigg\}. \qquad \text{(A16)}
\end{aligned}
$$

APPENDIX B: PARTIAL WAVE EXPANSION

Expressions of the Born kernel $\langle \boldsymbol{k}'_1\sigma'_1\tau'_1,-\boldsymbol{k}'_1\sigma'_2\tau'_2|V_{12(3)}|\boldsymbol{k}_1\sigma_1\tau_1,-\boldsymbol{k}_1\sigma_2\tau_2\rangle$ in the previous section need to be expanded into partial waves for standard nuclear-matter G-matrix calculations. The procedure may be found in Ref. [29]. I use the abbreviated notations for integrals involving second kind Legendre functions Q_ℓ's:

$$Q^\ell_{W0}(k'_1,k_1) \equiv \frac{1}{(2\pi)^2}\frac{1}{2}\int_0^{k_F} dk_3\, Q_\ell(x')Q_\ell(x), \tag{B1}$$

$$Q^\ell_{W2}(k'_1,k_1) \equiv \frac{1}{(2\pi)^2}\frac{1}{2k'_1k_1}\int_0^{k_F} dk_3 k_3^2\, Q_\ell(x')Q_\ell(x), \tag{B2}$$

$$Q^\ell_{W4}(k'_1,k_1) \equiv \frac{1}{(2\pi)^2}\frac{1}{2(k'_1k_1)^2}\int_0^{k_F} dk_3 k_3^4\, Q_\ell(x')Q_\ell(x), \tag{B3}$$

$$Q^\ell_{W1}(k'_1,k_1) \equiv \frac{1}{(2\pi)^2}\frac{1}{2k_1}\int_0^{k_F} dk_3 k_3 x'\, Q_\ell(x')Q_\ell(x), \tag{B4}$$

$$Q^\ell_{W1}(k_1,k'_1) \equiv \frac{1}{(2\pi)^2}\frac{1}{2k'_1}\int_0^{k_F} dk_3 k_3 x\, Q_\ell(x')Q_\ell(x), \tag{B5}$$

where $x \equiv \frac{k_1^2+k_3^2+m_\pi^2}{2k_1k_3}$ and $x' \equiv \frac{k_1'^2+k_3^2+m_\pi^2}{2k'_1k_3}$.

The central component of the c_1 interaction of V_C, Eq. (A8), with an orbital angular momentum ℓ is

$$\begin{aligned}
&\frac{c_1g_A^2m_\pi^2\rho_0}{f_\pi^4}\frac{1}{3}(\boldsymbol{\sigma}_1\cdot\boldsymbol{\sigma}_2)(\boldsymbol{\tau}_1\cdot\boldsymbol{\tau}_2)\left(\frac{1}{2k'_1k_1}Q_\ell(z)+\frac{m_\pi^2}{(2k'_1k_1)^2}Q_\ell{}'(z)\right)\\
&-\frac{2}{3}\frac{c_1g_A^2m_\pi^2}{f_\pi^4}(\boldsymbol{\sigma}_1\cdot\boldsymbol{\sigma}_2)(\boldsymbol{\tau}_1\cdot\boldsymbol{\tau}_2)\left\{\frac{1}{2k'_1k_1}Q_\ell(z)\big(\boldsymbol{k}_1'^2(F_0(k'_1)-F_1(k'_1))+\boldsymbol{k}_1^2(F_0(k_1)-F_1(k_1))\big)\right.\\
&\left.-\frac{1}{2}Q^{(1)}_\ell(z)(F_0(k'_1)+F_0(k_1)-F_1(k'_1)-F_1(k_1))\right\}-6\frac{c_1g_A^2m_\pi^2}{f_\pi^4}\left(\delta_{\ell0}\frac{1}{2}(F_0(k'_1)+F_0(k_1))\right.\\
&\left.+\frac{\ell+1}{2\ell+1}Q^{\ell+1}_{W0}(k'_1,k_1)+\frac{\ell}{2\ell+1}Q^{\ell-1}_{W0}(k'_1,k_1)+Q^\ell_{W2}(k'_1,k_1)-Q^\ell_{W1}(k'_1,k_1)-Q^\ell_{W1}(k_1,k'_1)\right).
\end{aligned} \tag{B6}$$

The tensor components of the c_1 interaction of V_C, Eq. (A8), are

$$\begin{aligned}
&\frac{c_1g_A^2m_\pi^2\rho_0}{f_\pi^4}\frac{1}{3}(\boldsymbol{\tau}_1\cdot\boldsymbol{\tau}_2)(S_{12})^{\ell'}_{\ell1J}\frac{-1}{2k'_1k_1}\left(k_1'^2\frac{1}{2k'_1k_1}Q'_\ell(z)+k_1^2\frac{1}{2k'_1k_1}Q'_{\ell'}(z)-Q'_J(z)\right)-\frac{2}{3}\frac{c_1g_A^2m_\pi^2}{f_\pi^4}(\boldsymbol{\tau}_1\cdot\boldsymbol{\tau}_2)(S_{12})^{\ell'}_{\ell1J}\\
&\times\left(\frac{k_1^2}{2k'_1k_1}Q_{\ell'}(z)(F_0(k'_1)-F_1(k'_1))+\frac{k_1'^2}{2k'_1k_1}Q_\ell(z)(F_0(k_1)-F_1(k_1))-\frac{1}{2}Q_J(z)(F_0(k'_1)+F_0(k_1)-F_1(k'_1)-F_1(k_1))\right)
\end{aligned} \tag{B7}$$

for $\ell' = \ell\pm2$ ($J=\ell\pm1$) and

$$\begin{aligned}
&\frac{c_1g_A^2m_\pi^2\rho_0}{f_\pi^4}\frac{1}{3}(\boldsymbol{\tau}_1\cdot\boldsymbol{\tau}_2)(S_{12})^{\ell'}_{\ell1J}\frac{-1}{2k'_1k_1}\left\{k_1'^2\frac{1}{2k'_1k_1}Q'_\ell(z)+k_1^2\frac{1}{2k'_1k_1}Q'_{\ell'}(z)-\frac{1}{2}\left(\frac{2\ell+3}{2\ell+1}Q'_{\ell-1}(z)+\frac{2\ell-1}{2\ell+1}Q'_{\ell+1}(z)\right)\right\}\\
&-\frac{2}{3}\frac{c_1g_A^2m_\pi^2}{f_\pi^4}(\boldsymbol{\tau}_1\cdot\boldsymbol{\tau}_2)(S_{12})^{\ell'}_{\ell1J}\left\{\frac{k_1^2}{2k'_1k_1}Q_{\ell'}(z)(F_0(k'_1)-F_1(k'_1))+\frac{k_1'^2}{2k'_1k_1}Q_\ell(z)(F_0(k_1)-F_1(k_1))\right.\\
&\left.-\frac{1}{2}\left(\frac{2\ell+3}{2\ell+1}Q_{\ell-1}(z)+\frac{2\ell-1}{2\ell+1}Q_{\ell+1}(z)\right)(F_0(k'_1)+F_0(k_1)-F_1(k'_1)-F_1(k_1))\right\}.
\end{aligned} \tag{B8}$$

for $\ell' = \ell = J\pm1$. The spin-orbit component of the c_1 term of V_C, Eq. (A8), becomes

$$\delta_{S1}\frac{c_1g_A^2m_\pi^2}{f_\pi^4}3\frac{\ell(\ell+1)+2-J(J+1)}{2\ell+1}\left\{-Q^{\ell-1}_{W0}(k'_1,k_1)+Q^{\ell+1}_{W0}(k'_1,k_1)+W^\ell_{\ell s,0}(k'_1,k_1)\right\}, \tag{B9}$$

where the function $W^\ell_{\ell s,0}(k'_1,k_1)$ is defined as

$$W^\ell_{\ell s,0}(k'_1,k_1) = \frac{4\pi}{(2\pi)^3}\int_0^\infty dk_3\frac{k_3}{4k'_1k_1}\{k'_1Q_\ell(x)(Q_{\ell-1}(x')-Q_{\ell+1}(x'))+k_1Q_\ell(x)(Q_{\ell-1}(x)-Q_{\ell+1}(x))\}. \tag{B10}$$

The central component of the c_3 interaction of V_C, Eq. (A9), is

$$\begin{aligned}
&\frac{c_3 g_A^2 \rho_0}{2 f_\pi^4}\frac{1}{3}(\boldsymbol{\sigma}_1\cdot\boldsymbol{\sigma}_2)(\boldsymbol{\tau}_1\cdot\boldsymbol{\tau}_2)\left\{\delta_{\ell 0}-\frac{m_\pi^2}{k_1' k_1}Q_\ell(z)+\left(\frac{m_\pi^2}{2k_1' k_1}\right)^2\frac{\ell+1}{z^2-1}(zQ_\ell(z)-Q_{\ell+1}(z))\right\}\\
&-\frac{c_3 g_A^2}{2 f_\pi^4}\frac{2}{3}(\boldsymbol{\tau}_1\cdot\boldsymbol{\tau}_2)(\boldsymbol{\sigma}_1\cdot\boldsymbol{\sigma}_2)\left\{\frac{1}{3}\left[\delta_{\ell 0}-m_\pi^2\frac{1}{2k_1' k_1}Q_\ell(z)\right]\left(k_1^2F_2(k_1)+k_1'^2F_2(k_1')\right)\right.\\
&+\left[-\frac{1}{2}k_1' k_1\frac{1}{3}\delta_{\ell 1}-\frac{1}{4}\left(k_1'^2-3k_1^2+m_\pi^2\right)\delta_{\ell 0}+\frac{1}{4}\left(k_1'^2-k_1^2+m_\pi^2\right)^2\frac{1}{2k_1' k_1}Q_\ell(z)\right](F_0(k_1)-2F_1(k_1))\\
&+\left[-\frac{1}{2}k_1' k_1\frac{1}{3}\delta_{\ell 1}-\frac{1}{4}\left(k_1^2-3k_1'^2+m_\pi^2\right)\delta_{\ell 0}+\frac{1}{4}\left(k_1^2-k_1'^2+m_\pi^2\right)^2\frac{1}{2k_1' k_1}Q_\ell(z)\right](F_0(k_1')-2F_1(k_1'))\\
&+\left[-\frac{k_1'^2}{6k_1' k_1}\delta_{\ell 1}-\frac{1}{2k_1' k_1}\left[\frac{k_1'^2}{2k_1' k_1}\left(k_1'^2+k_1^2+m_\pi^2\right)-\frac{4}{3}k_1' k_1\right]\delta_{\ell 0}\right.\\
&+\left[\left(\frac{k_1'}{2k_1' k_1}\right)^2\left(k_1'^2+k_1^2+m_\pi^2\right)^2-k_1'^2-\frac{2}{3}m_\pi^2\right]\frac{1}{2k_1' k_1}Q_\ell(z)\Big]k_1^2F_3(k_1)\\
&+\left[-\frac{k_1^2}{6k_1' k_1}\delta_{\ell 1}-\frac{1}{2k_1' k_1}\left[\frac{k_1^2}{2k_1' k_1}\left(k_1'^2+k_1^2+m_\pi^2\right)-\frac{4}{3}k_1' k_1\right]\delta_{\ell 0}\right.\\
&+\left[\left(\frac{k_1}{2k_1' k_1}\right)^2\left(k_1'^2+k_1^2+m_\pi^2\right)^2-k_1^2-\frac{2}{3}m_\pi^2\right]\frac{1}{2k_1' k_1}Q_\ell(z)\Big]k_1'^2F_3(k_1')\\
&-\frac{c_3 g_A^2}{2 f_\pi^4}6\left\{\delta_{\ell 0}\left[\frac{1}{8}\rho_0-\left(\frac{3}{4}m_\pi^2+\frac{1}{2}k_1'^2+\frac{1}{4}k_1^2\right)F_0(k_1')-\left(\frac{3}{4}m_\pi^2+\frac{1}{2}k_1^2+\frac{1}{4}k_1'^2\right)F_0(k_1)\right.\right.\\
&\left.+\frac{1}{4}\left(k_1'^2F_2(k_1')+k_1^2F_2(k_1)\right)\right]+\delta_{\ell 1}\frac{k_1' k_1}{3}\left[F_0(k_1')+F_0(k_1)-\frac{1}{2}(F_1(k_1')+F_1(k_1))\right]\\
&+\frac{1}{4k_1' k_1}\left(k_1'^2+k_1^2+2m_\pi^2\right)^2Q_{W0}^{\ell}(k_1',k_1)-\left(k_1'^2+k_1^2+2m_\pi^2\right)\left(\frac{\ell}{\hat{\ell}}Q_{W0}^{\ell-1}(k_1',k_1)+\frac{(\ell+1)}{\hat{\ell}}Q_{W0}^{\ell+1}(k_1,k_1')\right)\\
&\left.+\frac{k_1' k_1}{\hat{\ell}}\left[\frac{(\ell+1)(\ell+2)}{2\ell+3}Q_{W0}^{\ell+2}(k_1',k_1)+\left(\frac{\ell^2}{2\ell-1}+\frac{(\ell+1)^2}{2\ell+3}\right)Q_{W0}^{\ell}(k_1',k_1)+\frac{\ell(\ell-1)}{2\ell-1}Q_{W0}^{\ell-2}(k_1',k_1)\right]\right\}. \qquad \text{(B11)}
\end{aligned}$$

The tensor components of the c_3 interaction of V_C, Eq. (A8), are

$$\begin{aligned}
&\frac{c_3 g_A^2}{2 f_\pi^4}(S_{12})^{\ell'}_{\ell 1 J}\frac{\rho_0}{3}(\boldsymbol{\tau}_1\cdot\boldsymbol{\tau}_2)\left[\frac{k_1'^2}{2k_1' k_1}\left(Q_\ell(z)+\frac{m_\pi^2}{2k_1' k_1}Q'_\ell(z)\right)+\frac{k_1^2}{2k_1' k_1}\left(Q_{\ell'}(z)+\frac{m_\pi^2}{2k_1' k_1}Q'_{\ell'}(z)\right)-\left(Q_J(z)+\frac{m_\pi^2}{2k_1' k_1}Q'_J(z)\right)\right]\\
&-\frac{c_3 g_A^2}{2 f_\pi^4}\frac{2}{3}(\boldsymbol{\tau}_1\cdot\boldsymbol{\tau}_2)\left[(F_0(k_1)-2F_1(k_1))\left\{-k_1^2\left(\frac{1}{2}Q^{(1)}_{\ell'}(z)-\frac{k_1^2}{2k_1' k_1}Q_{\ell'}(z)\right)+k_1' k_1\left(\frac{1}{2}Q^{(1)}_{J}(z)-\frac{k_1^2}{2k_1' k_1}Q_J(z)\right)\right\}\right.\\
&+(F_0(k_1')-2F_1(k_1'))\left\{k_1'^2\left(-\frac{1}{2}Q^{(1)}_{\ell}(z)+\frac{k_1'^2}{2k_1' k_1}Q_\ell(z)\right)-k_1' k_1\left(-\frac{1}{2}Q^{(1)}_{J}(z)+\frac{k_1'^2}{2k_1' k_1}Q_J(z)\right)\right\}\\
&+\frac{1}{3}\left(k_1'^2F_2(k_1')+k_1^2F_2(k_1)\right)\left\{\frac{k_1'^2}{2k_1' k_1}Q_\ell(z)+\frac{k_1^2}{2k_1' k_1}Q_{\ell'}(z)-Q_J(z)\right\}+\frac{1}{3}\left(2k_1^2F_3(k_1)-k_1'^2F_3(k_1')\right)\frac{k_1^2}{2k_1' k_1}Q_{\ell'}(z)\\
&-\frac{1}{2}k_1^2F_3(k_1)Q^{(1)}_{\ell'}(z)+\frac{1}{3}\left(2k_1'^2F_3(k_1')-k_1^2F_3(k_1)\right)\frac{k_1'^2}{2k_1' k_1}Q_\ell(z)-\frac{1}{2}k_1'^2F_3(k_1')Q^{(1)}_{\ell}(z)\\
&\left.-\frac{1}{3}\left(k_1^2F_3(k_1)+k_1'^2F_3(k_1')\right)\frac{1}{2}Q_J(z)+\frac{1}{2}k_1' k_1(F_3(k_1')+F_3(k_1))Q^{(1)}_{J}(z)\right] \qquad \text{(B12)}
\end{aligned}$$

for $\ell'=\ell\pm 2$ ($J=\ell\pm 1$) and

$$\begin{aligned}
&\frac{c_3 g_A^2}{2 f_\pi^4}(S_{12})^{\ell'}_{\ell 1 J}\frac{\rho_0}{3}(\boldsymbol{\tau}_1\cdot\boldsymbol{\tau}_2)\left[\frac{k_1'^2+k_1^2}{2k_1' k_1}\left(Q_\ell(z)+\frac{m_\pi^2}{2k_1' k_1}Q'_\ell(z)\right)\right.\\
&\left.-\frac{1}{2}\left\{\frac{2\ell+3}{2\ell+1}\left(Q_{\ell-1}(z)+\frac{m_\pi^2}{2k_1' k_1}Q'_{\ell-1}(z)\right)+\frac{2\ell-1}{2\ell+1}\left(Q_{\ell+1}(z)+\frac{m_\pi^2}{2k_1' k_1}Q'_{\ell+1}(z)\right)\right\}\right]
\end{aligned}$$

$$
\begin{aligned}
&- \frac{c_3 g_A^2}{2f_\pi^4}\frac{2}{3}(\boldsymbol{\tau}_1\cdot\boldsymbol{\tau}_2)\Bigg[(F_0(k_1)-2F_1(k_1))\Bigg\{-k_1^2\left(\frac{1}{2}Q_\ell^{(1)}(z)-\frac{k_1^2}{2k_1'k_1}Q_\ell(z)\right)\\
&+\frac{1}{2}k_1'k_1\left(\frac{2\ell+3}{2\ell+1}\left(\frac{1}{2}Q_{\ell-1}^{(1)}(z)-\frac{k_1^2}{2k_1'k_1}Q_{\ell-1}(z)\right)+\frac{2\ell-1}{2\ell+1}\left(\frac{1}{2}Q_{\ell+1}^{(1)}(z)-\frac{k_1^2}{2k_1'k_1}Q_{\ell+1}(z)\right)\right)\Bigg\}\\
&+(F_0(k_1')-2F_1(k_1'))\Bigg\{k_1'^2\left(-\frac{1}{2}Q_\ell^{(1)}(z)+\frac{k_1'^2}{2k_1'k_1}Q_\ell(z)\right)\\
&+\frac{1}{2}k_1'k_1\left(\frac{2\ell+3}{2\ell+1}\left(\frac{1}{2}Q_{\ell-1}^{(1)}(z)-\frac{k_1'^2}{2k_1'k_1}Q_{\ell-1}(z)\right)+\frac{2\ell-1}{2\ell+1}\left(\frac{1}{2}Q_{\ell+1}^{(1)}(z)-\frac{k_1'^2}{2k_1'k_1}Q_{\ell+1}(z)\right)\right)\Bigg\}\\
&+\frac{1}{3}\left(2k_1^2F_3(k_1)-k_1'^2F_3(k_1')\right)\frac{k_1^2}{2k_1'k_1}Q_\ell(z)-\frac{1}{2}k_1^2F_3(k_1)Q_\ell^{(1)}(z)+\frac{1}{3}\left(2k_1'^2F_3(k_1')-k_1^2F_3(k_1)\right)\frac{k_1'^2}{2k_1'k_1}Q_\ell(z)\\
&-\frac{1}{2}k_1'^2F_3(k_1')Q_\ell^{(1)}(z)-\frac{1}{3}\left(k_1^2F_3(k_1)+k_1'^2F_3(k_1')\right)\frac{1}{4}\left\{\frac{2\ell+3}{2\ell+1}Q_{\ell-1}(z)+\frac{2\ell-1}{2\ell+1}Q_{\ell+1}(z)\right\}\\
&+k_1'k_1(F_3(k_1')+F_3(k_1'))\frac{1}{4}\left\{\frac{2\ell+3}{2\ell+1}Q_{\ell-1}^{(1)}(z)+\frac{2\ell-1}{2\ell+1}Q_{\ell+1}^{(1)}(z)\right\}\Bigg] \qquad \text{(B13)}
\end{aligned}
$$

for $\ell'=\ell=J\pm1$. The spin-orbit component of the c_3 term of V_C, Eq. (A9), becomes

$$
\begin{aligned}
&\delta_{S1}\frac{c_3 g_A^2}{2f_\pi^4}3\frac{\ell(\ell+1)+2-J(J+1)}{2\ell+1}\Bigg[\left(m_\pi^2+\frac{1}{2}\left(k_1'^2+k_1^2\right)\right)\left\{Q_{W0}^{\ell-1}(k_1',k_1)-Q_{W0}^{\ell+1}(k_1',k_1)-W_{\ell s,0}^{\ell}(k_1',k_1)\right\}\\
&-\delta_{\ell 1}\frac{k_1'k_1}{2}(F_0(k_1')+F_0(k_1)-F_1(k_1')-F_1(K_1))+6\frac{k_1'k_1}{2}\left\{\frac{\ell-1}{2\ell-1}W_{\ell s,0}^{\ell-1}(k_1',k_1)+\frac{\ell+2}{2\ell+3}W_{\ell s,0}^{\ell+1}(k_1',k_1)\right\}\Bigg]. \qquad \text{(B14)}
\end{aligned}
$$

The central component of the c_4 interaction of V_C, Eq. (A10), is

$$
\begin{aligned}
&2\frac{c_4 g_A^2}{4f_\pi^4}\frac{2}{3}(\boldsymbol{\sigma}_1\cdot\boldsymbol{\sigma}_2)(\boldsymbol{\tau}_1\cdot\boldsymbol{\tau}_2)\Bigg[\left(\frac{1}{2}\rho_0-m_\pi^2(F_0(k_1')+F_0(k_1))-\frac{1}{3}\left(k_1'^2F_2(k_1')+k_1^2F_2(k_1)\right)\right)\left(\delta_{\ell 0}-\frac{m_\pi^2}{2k_1'k_1}Q_\ell(z)\right)\\
&+(F_0(k_1')-2F_1(k_1'))\left(\frac{1}{4}\left(k_1^2-3k_1'^2+m_\pi^2\right)\delta_{\ell 0}+\frac{1}{6}k_1'k_1\delta_{\ell 1}-\frac{1}{4}\left(k_1^2-k_1'^2+m_\pi^2\right)^2\frac{1}{2k_1'k_1}Q_\ell(z)\right)\\
&+(F_0(k_1)-2F_1(k_1))\left(\frac{1}{4}\left(k_1'^2-3k_1^2+m_\pi^2\right)\delta_{\ell 0}+\frac{1}{6}k_1'k_1\delta_{\ell 1}-\frac{1}{4}\left(k_1'^2-k_1^2+m_\pi^2\right)^2\frac{1}{2k_1'k_1}Q_\ell(z)\right)\\
&+\left[\left\{\frac{1}{4}\left(k_1'^2+k_1^2+m_\pi^2\right)-\frac{2}{3}k_1'^2\right\}\delta_{\ell 0}+\frac{1}{6}k_1'k_1\delta_{\ell 1}-\left\{\frac{1}{4}\left(k_1'^2+k_1^2+m_\pi^2\right)^2-k_1'^2k_1^2-\frac{2}{3}m_\pi^2k_1'^2\right\}\frac{1}{2k_1'k_1}Q_\ell(z)\right]F_3(k_1')\\
&+\left[\left\{\frac{1}{4}\left(k_1'^2+k_1^2+m_\pi^2\right)-\frac{2}{3}k_1^2\right\}\delta_{\ell 0}+\frac{1}{6}k_1'k_1\delta_{\ell 1}-\left\{\frac{1}{4}\left(k_1'^2+k_1^2+m_\pi^2\right)^2-k_1'^2k_1^2-\frac{2}{3}m_\pi^2k_1^2\right\}\frac{1}{2k_1'k_1}Q_\ell(z)\right]F_3(k_1)\\
&+\delta_{\ell 0}\left\{\frac{1}{8}\rho_0+\frac{1}{4}\left(2k_1'^2+k_1^2-m_\pi^2\right)F_0(k_1')+\frac{1}{4}\left(k_1'^2+2k_1^2-m_\pi^2\right)F_0(k_1)-\frac{1}{4}\left(k_1'^2F_2(k_1')+k_1^2F_2(k_1)\right)\right\}\\
&+\delta_{\ell 1}k_1'k_1\left\{\frac{1}{6}(F_1(k_1')+F_1(k_2))-\frac{1}{3}(F_0(k_1')+F_0(k_1))\right\}-\frac{1}{4}\left(k_1'^2+k_1^2\right)\left(k_1'^2+k_1^2+4m_\pi^2\right)\frac{1}{k_1'k_1}Q_{W0}^{\ell}(k_1',k_1)\\
&+\left(k_1'^2+k_1^2+2m_\pi^2\right)\frac{1}{2\ell+1}\left[\ell Q_{W0}^{\ell-1}(k_1',k_1)+(\ell+1)Q_{W0}^{\ell+1}(k_1',k_1)\right]\\
&-k_1'k_1\frac{1}{2\ell+1}\left\{\frac{(\ell-1)\ell}{2\ell-1}Q_{W0}^{\ell-2}(k_1',k_1)+\left(\frac{(\ell+1)^2}{2\ell+3}+\frac{\ell^2}{2\ell-1}\right)Q_{W0}^{\ell}(k_1',k_1)+\frac{(\ell+2)(\ell+1)}{2\ell+3}Q_{W0}^{\ell+2}(k_1',k_1)\right\}\Bigg]. \qquad \text{(B15)}
\end{aligned}
$$

The tensor components of the c_4 interaction of V_C, Eq. (A10), are

$$
\begin{aligned}
&2\frac{c_4 g_A^2}{4f_\pi^4}\frac{2}{3}(S_{12})_{\ell 1 J}^{\ell'}(\boldsymbol{\tau}_1\cdot\boldsymbol{\tau}_2)\Bigg[\frac{1}{2k_1'k_1}\left(k_1'^2Q_\ell(z)+k_1^2Q_{\ell'}(z)-2k_1'k_1Q_J(z)\right)\left(\frac{1}{2}\rho_0-m_\pi^2(F_0(K_1')+F_0(k_1))\right)\\
&+\frac{k_1'k_1}{2J+1}\left(Q_{W0}^{J+1}(k_1',k_1)-Q_{W0}^{J-1}(k_1',k_1)\right)
\end{aligned}
$$

$$+(F_0(k_1')-2F_1(k_1'))\left\{\frac{k_1'^2}{4k_1'k_1}\left(-k_1'^2+k_1^2+m_\pi^2\right)Q_\ell(z)-\frac{1}{4}\left(-k_1'^2+k_1^2+m_\pi^2\right)Q_J(z)-k_1'^2\delta_{\ell 0}+\frac{1}{2}k_1'k_1\delta_{J0}\right\}$$

$$+(F_0(k_1)-2F_1(k_1))\left\{\frac{k_1^2}{4k_1'k_1}\left(k_1'^2-k_1^2+m_\pi^2\right)Q_{\ell'}(z)-\frac{1}{4}\left(k_1'^2-k_1^2+m_\pi^2\right)Q_J(z)-k_1^2\delta_{\ell 0}+\frac{1}{2}k_1'k_1\delta_{J0}\right\}$$

$$+\frac{1}{3}F_3(k_1')\left\{-\frac{3}{2}k_1'^2\delta_{\ell 0}+\frac{3}{2}k_1'k_1\delta_{J0}+\frac{k_1'^2}{4k_1'k_1}\left(-k_1'^2+3k_1^2+3m_\pi^2\right)Q_\ell(z)-\frac{1}{4}\left(k_1'^2+3k_1^2+3m_\pi^2\right)Q_J(z)+\frac{1}{2}k_1'k_1Q_{\ell'}(z)\right\}$$

$$+\frac{1}{3}F_3(k_1)\left\{-\frac{3}{2}k_1^2\delta_{\ell 0}+\frac{3}{2}k_1'k_1\delta_{J0}+\frac{k_1^2}{4k_1'k_1}\left(-k_1^2+3k_1'^2+3m_\pi^2\right)Q_{\ell'}(z)-\frac{1}{4}\left(k_1^2+3k_1'^2+3m_\pi^2\right)Q_J(z)+\frac{1}{2}k_1'k_1Q_\ell(z)\right\}$$

$$-\frac{1}{3}F_2(k_1')\frac{k_1'^4}{2k_1'k_1}Q_\ell(z)-\frac{1}{3}F_2(k_1)\frac{k_1^4}{2k_1'k_1}Q_{\ell'}(z)\Bigg] \tag{B16}$$

for $\ell'=\ell\pm 2$ ($J=\ell\pm 1$) and

$$2\frac{c_4g_A^2}{4f_\pi^4}\frac{2}{3}(S_{12})^{\ell'}_{\ell 1J}(\boldsymbol{\tau}_1\cdot\boldsymbol{\tau}_2)\Bigg[\left(\frac{1}{2}\rho_0-m_\pi^2(F_0(k_1')+F_0(k_1))\right)\left\{\frac{k_1^2+k_1'^2}{2k_1'k_1}Q_\ell(z)-\frac{1}{2}\frac{2\ell+3}{2\ell+1}Q_{\ell-1}(z)-\frac{1}{2}\frac{2\ell-1}{2\ell+1}Q_{\ell+1}(z)\right\}$$

$$+k_1'k_1\left\{\left(\frac{(2\ell+1)^2}{(2\ell-1)(2\ell+3)}-2\right)Q^\ell_{W0}(k_1',k_1)+\frac{(2\ell+3)(\ell-1)}{(2\ell+1)(2\ell-1)}Q^{\ell-2}_{W0}(k_1',k_1)+\frac{(2\ell-1)(\ell+1)}{(2\ell+1)(2\ell+3)}Q^{\ell+2}_{W0}(k_1',k_1)\right\}$$

$$+(F_0(k_1')-2F_1(k_1'))\left\{-\frac{1}{2}k_1'^2\delta_{\ell 0}+\frac{5}{12}k_1'k_1\delta_{\ell 1}+\frac{k_1'^2}{4k_1'k_1}\left(-k_1'^2+k_1^2+m_\pi^2\right)Q_\ell(z)\right.$$

$$\left.-\frac{1}{8(2\ell+1)}\left(-k_1'^2+k_1^2+m_\pi^2\right)((2\ell+3)Q_{\ell-1}(z)+(2\ell-1)Q_{\ell+1}(z))\right\}+\frac{1}{3}F_3(k_1')\left\{-\frac{3}{2}k_1'^2\delta_{\ell 0}+\frac{5}{4}k_1'k_1\delta_{\ell 1}\right.$$

$$\left.+\frac{k_1'^2}{4k_1'k_1}\left(-k_1'^2+5k_1^2+3m_\pi^2\right)Q_\ell(z)-\frac{1}{8(2\ell+1)}\left(k_1'^2+3k_1^2+3m_\pi^2\right)((2\ell+3)Q_{\ell-1}(z)+(2\ell-1)Q_{\ell+1}(z))\right\}$$

$$-\frac{1}{3}F_2(k_1')\frac{k_1'^4}{2k_1'k_1}Q_\ell(z)+(F_0(k_1)-2F_1(k_1))\left\{-\frac{1}{2}k_1^2\delta_{\ell 0}+\frac{5}{12}k_1'k_1\delta_{\ell 1}+\frac{k_1^2}{4k_1'k_1}\left(k_1'^2-k_1^2+m_\pi^2\right)Q_\ell(z)\right.$$

$$\left.-\frac{1}{8(2\ell+1)}\left(k_1'^2-k_1^2+m_\pi^2\right)((2\ell+3)Q_{\ell-1}(z)+(2\ell-1)Q_{\ell+1}(z))\right\}+\frac{1}{3}F_3(k_1)\left\{-\frac{3}{2}k_1^2\delta_{\ell 0}+\frac{5}{4}k_1'k_1\delta_{\ell 1}\right.$$

$$\left.+\frac{k_1^2}{4k_1'k_1}\left(-k_1^2+5k_1'^2+3m_\pi^2\right)Q_\ell(z)-\frac{1}{8(2\ell+1)}\left(k_1^2+3k_1'^2+3m_\pi^2\right)((2\ell+3)Q_{\ell-1}(z)+(2\ell-1)Q_{\ell+1}(z))\right\}$$

$$-\frac{1}{3}F_2(k_1)\frac{k_1^4}{2k_1'k_1}Q_\ell(z)\Bigg] \tag{B17}$$

for $\ell'=\ell=J\pm 1$. There is no spin-orbit component from the c_4 interaction of V_C, Eq. (A10).

The central component of the V_D interaction, Eq. (A11), is

$$\frac{g_A}{8f_\pi^2}\frac{c_D}{f_\pi^2\Lambda_\chi}\frac{1}{3}(\boldsymbol{\sigma}_1\cdot\boldsymbol{\sigma}_2)(\boldsymbol{\tau}_1\cdot\boldsymbol{\tau}_2)\left\{\frac{\rho_0m_\pi^2}{2k_1'k_1}Q_\ell(x)-\delta_{\ell 0}2m_\pi^2(F_0(k_1)+F_0(k_1'))\right\}+3\frac{g_A}{8f_\pi^2}\frac{c_D}{f_\pi^2\Lambda_\chi}\delta_{\ell 0}\left\{\rho_0-2m_\pi^2(F_0(k_1)+F_0(k_1'))\right\}. \tag{B18}$$

The tensor component for the initial ℓ and the final $\ell'=\ell\pm 1$ ($J=\ell\pm 1$) becomes

$$2\frac{g_A}{8f_\pi^2}\frac{c_D}{f_\pi^2\Lambda_\chi}(\boldsymbol{\tau}_1\cdot\boldsymbol{\tau}_2)\frac{1}{3}S_{12}\{F_0(k_1)-2F_1(k_1)+F_3(k_1)+F_0(k_1')-2F_1(k_1')+F_3(k_1')\}\left(k_1'^2\delta_{\ell 0}+k_1^2\delta_{\ell' 0}-2k_1'k_1\delta_{J0}\right)$$

$$-\frac{g_A}{8f_\pi^2}\frac{c_D\rho_0}{f_\pi^2\Lambda_\chi}(\boldsymbol{\tau}_1\cdot\boldsymbol{\tau}_2)\frac{1}{3}S_{12}\left\{\frac{k_1'^2}{2k_1'k_1}Q_\ell(x)+\frac{k_1^2}{2k_1'k_1}Q_{\ell'}(x)-Q_J(x)\right\}, \tag{B19}$$

and for $\ell' = \ell = J, J \pm 1$

$$2\frac{g_A}{8f_\pi^2}\frac{c_D}{f_\pi^2\Lambda_\chi}(\boldsymbol{\tau}_1\cdot\boldsymbol{\tau}_2)\frac{1}{3}(S_{12})^{\ell'}_{\ell 1 J}\{F_0(k_1)-2F_1(k_1)+F_3(k_1)+F_0(k_1')-2F_1(k_1')+F_3(k_1')\}\left\{k_1'^2\delta_{\ell 0}+k_1^2\delta_{\ell' 0}-\frac{5}{3}k_1'k_1\delta_{\ell 1}\right\}$$
$$-\frac{g_A}{8f_\pi^2}\frac{c_D\rho_0}{f_\pi^2\Lambda_\chi}(\boldsymbol{\tau}_1\cdot\boldsymbol{\tau}_2)\frac{1}{3}S_{12}\left\{\frac{k_1'^2}{2k_1'k_1}Q_\ell(x)+\frac{k_1^2}{2k_1'k_1}Q_{\ell'}(x)-\frac{1}{2}\left(\frac{2\ell+3}{2\ell+1}Q_{\ell-1}(z)+\frac{2\ell-1}{2\ell+1}Q_{\ell+1}(z)\right)\right\}. \quad \text{(B20)}$$

There is no spin-orbit component from the c_4 interaction of V_D, Eq. (A11).

Finally, the V_E interaction, Eq. (A12), gives only an $\ell = 0$ central component; namely, $-6\frac{C_E\frac{1}{4}\rho_0}{f_\pi^4\Lambda_\chi}$ both for $^1S_0$ and $^3S_1$ channels.

[1] K. A. Brueckner, C. A. Levinson, and H. M. Mahmoud, Phys. Rev. **95**, 217 (1954).
[2] B. D. Day, Rev. Mod. Phys. **39**, 719 (1967).
[3] H. A. Bethe, Ann. Rev. Nucl. Sci. **21**, 93 (1971).
[4] V. R. Pandharipande and R. B. Wiringa, Rev. Mod. Phys. **51**, 821 (1979).
[5] M. Baldo and G. F. Burgio, Rep. Prog. Phys. **75**, 026301 (2012).
[6] R. Brockmann and R. Machleidt, Phys. Rev. C **42**, 1965 (1990).
[7] R. Machleidt and D. R. Entem, Phys. Rep. **503**, 1 (2011).
[8] E. Epelbaum, W. Göckle, and U.-G. Meißner, Nucl. Phys. A **747**, 362 (2005).
[9] E. Epelbaum, H.-W. Hammer, and U.-G. Meißner, Rev. Mod. Phys. **81**, 1773 (2009).
[10] A. Klein, Phys. Rev. **90**, 1101 (1953).
[11] J. Fujita and H. Miyazawa, Prog. Theor. Phys **17**, 366 (1957).
[12] R. B. Wiringa, S. C. Pieper, J. Carlson, and V. R. Pandharipande, Phys. Rev. C **62**, 014001 (2000).
[13] N. Kalantar-Nayestanaki, E. Epelbaum, J. G. Messchendorp, and A. Nogga, Rep. Prog. Phys. **75**, 016301 (2012).
[14] T. Kasahara, Y. Akaishi, and H. Tanaka, Prog. Theor. Phys. Suppl. **56**, 96 (1974).
[15] B. Friedman and V. R. Pandharipande, Nucl. Phys. A **361**, 502 (1981).
[16] A. Akmal, V. R. Pandharipande, and D. G. Ravenhall, Phys. Rev. C **58**, 1804 (1998).
[17] S. K. Bogner, A. Schwenk, R. J. Furnstahl, and A. Nogga, Nucl. Phys. A **763**, 59 (2005).
[18] K. Hebeler, S. K. Bogner, R. J. Furnstahl, A. Nogga, and A. Schwenk, Phys. Rev. C **83**, 031301(R) (2011).
[19] K. Hebeler and A. Schwenk, Phys. Rev. C **82**, 014314 (2010).
[20] I. Tews, T. Krüger, K. Hebeler, and A. Schwenk, Phys. Rev. Lett. **110**, 032504 (2013).
[21] L. Coraggio, J. W. Holt, N. Itaco, R. Machleidt, and F. Sammarruca, Phys. Rev. C **87**, 014322 (2013).
[22] M. Kohno, Phys. Rev. C **86**, 061301(R) (2012).
[23] F. Sammarruca, B. Chen, L. Coraggio, N. Itaco, and R. Machleidt, Phys. Rev. C **86**, 054317 (2012).
[24] B. A. Loiseau, Y. Nogami, and C. K. Ross, Nucl. Phys. A **165**, 601 (1971); **176**, 665 (1971).
[25] J. W. Holt, N. Kaiser, and W. Weise, Phys. Rev. C **81**, 024002 (2010).
[26] M. Kohno and R. Okamoto, Phys. Rev. C **86**, 014317 (2012).
[27] M. I. Haftel and F. Tabakin, Nucl. Phys. A **158**, 1 (1970).
[28] K. Suzuki, R. Okamoto, M. Kohno, and S. Nagata, Nucl. Phys. A **665**, 92 (2000).
[29] Y. Fujiwara, M. Kohno, T. Fujita, C. Nakamoto, and Y. Suzuki, Prog. Theor. Phys. **103**, 755 (2000).
[30] R. B. Wiringa, V. G. J. Stoks, and R. Schiavilla, Phys. Rev. C **51**, 38 (1995).
[31] T. A. Rijken, V. G. J. Stoks, and Y. Yamamoto, Phys. Rev. C **59**, 21 (1999).
[32] R. Machleidt, Phys. Rev. C **63**, 024001 (2001).
[33] D. Gogny and R. Padjen, Nucl. Phys. A **293**, 365 (1977).
[34] T. Sasaki, N. Yasutake, M. Kohno, H. Kouno, and M. Yahiro, arXiv:1307.0681.
[35] A. Bohr and B. Mottelson, *Nuclear Structure*, Vol. I (Benjamin, Reading, MA, 1969).
[36] T. Shoji and Y. R. Shimizu, Prog. Theor. Phys. **121**, 319 (2009).